Modeling the behaviour of sulfur in magmatic systems from source to surface: Application to Whakaari/White Island, Aotearoa New Zealand, and Etna, Italy

Ery C. Hughes: Te Pū Ao | GNS Science (e.hughes@gns.cri.nz)

Joseph Biasi: University of Wyoming

Isabel Fendley: Pennsylvania State University

Kristen Rahilly: Oregon State University

Tyler Schlieder: Pacific Northwest National Laboratory

Heather Winslow: University of Nevada

Tobias P. Fischer: University of New Mexico

Paul Wallace: University of Oregon

Twitter handles: @eryhughes, @izzifen, @kristen_rahilly, @HeatherBWinslow

Abstract

Our understanding of the role of volcanoes in the global sulfur cycle and how volcanic gas emissions can be used to monitor volcanoes is limited by the complex interactions between hydrothermal systems and volcanic sulfur emissions. Hydrothermal systems influence the amount and speciation of volcanogenic sulfur, which is ultimately released to the surface/atmosphere via a range of physicochemical processes. To understand the effect of the hydrothermal system, on surface emissions we model the magmatic-hydrothermal systems at Whakaari/White Island, Aotearoa New Zealand, and Etna, Italy. We quantify the magmatic sulfur inputs using mass balance and MELTS modeling (thermodynamic model of crystallization); model the effects of degassing using Sulfur_X (an empirical model of melt-gas equilibria); and model the influence of the hydrothermal system using CHIM-XPT and EQ3/6 (thermodynamic and kinetic models of gas+water±rock reactions), which we compare to measured plume and fumarole compositions. We find that the sulfur inputs can broadly equal sulfur outputs over long timescales. However, the hydrothermal system can modulate the total mass of sulfur released and its H_2S/SO_2 ratio on shorter timescales, especially as the system evolves from water- to gas-dominated through the development of dry, gas-dominated pathways.

Keywords: sulfur, Whakaari, Etna, hydrothermal systems, degassing

1 Introduction

Volcanoes are a critical component of the global sulfur cycle; therefore, a robust understanding of the journey of sulfur through volcanic systems is needed (e.g., Kagoshima et al., 2015). However, the behavior of sulfur within magmatic systems from source (parent magma) to surface (outgassing) is difficult to constrain due to the wide range of potential oxidation states, species, and phases sulfur can be present in (e.g., Baker & Moretti, 2011, Moretti & Stefansson, 2020; Cicconi et al., 2020). In particular, the role of hydrothermal "scrubbing" in modulating the eventual output of sulfur at the surface is important to constrain (e.g., Symonds et al., 2001; de Moor et al., 2019; Christenson et al, 2017; Fischer et al., 2015). Following Symonds et al. (2001), we use a broad definition for "scrubbing", which refers to the removal of sulfur from volcanic gas through reactions with water±rock in the hydrothermal system (i.e., both hydrolysis of SO_2 to H_2S and precipitation of sulfur-bearing minerals).

Changes in the flux and composition of gases emitted at volcanoes are an integral part of volcano monitoring efforts as they are an indicator of magmatic input and can suggest increased likelihood of eruption (recent examples from: Werner et al., 2011; Patane et al., 2013; de Moor et al., 2016a; Aiuppa et al., 2017). The combination of absolute S and CO_2 fluxes with C/S ratios is particularly useful for interpreting the magmatic system because CO_2 and S fractionate during degassing and hydrothermal interactions. CO_2 is less soluble than S in silicate melts, causing CO_2 to exsolve into a gas phase at higher pressures (P) than S (e.g., Shinohara et al., 2008; Lesne et al., 2011; Lopez et al., 2018). CO_2 is also less soluble than S in hydrothermal waters; hence, CO_2 does not react with hydrothermal waters, unlike S (e.g., Symonds et al., 2001; de Moor et al., 2016b). SO_2 is easily measured using ground- and space-based techniques due to its low background abundance in the atmosphere (e.g., Carn et al., 2017). The CO_2 flux can then be estimated using the measured sulfur flux and C/S ratio of the gas (e.g., Allard 1991; Williams et al., 1992; Fischer et al., 2019).

Here we constrain sulfur inputs, outputs, and extent of hydrothermal scrubbing including the effects of shallow water scrubbing through the presence of a crater lake for two

volcanoes with active hydrothermal systems using quantitative models. We choose Whakaari/White Island, Aotearoa New Zealand (referred to as Whakaari throughout), and Etna, Italy, as case studies. Importantly, both have abundant published and/or freely accessible monitoring data on the flux and composition of the melt and gas within the volcanic systems. Comparing these volcanic systems allows us to understand the effectiveness of our modeling approach for systems with different compositions and sub-surface architectures. We use these case studies to: (1) evaluate whether the sulfur flux at the surface can be balanced by the sulfur flux derived from the parent magma into the system, and (2) quantify how the presence of a hydrothermal system affects the sulfur emission at the surface.

Magmatic sulfur inputs were determined using a combination of whole-rock and melt-inclusion data; edifice volumes and ages; crystallization modeling using MELTS (Asimow & Ghiorso 1998; Ghiorso et al. 2002); and using a range of intrusive to extrusive magma volume estimates. The process of degassing on melt and gas chemical composition was modeled using Sulfur_X (Ding et al., 2023). To model the effects of the hydrothermal system, we use EQ3/6 geochemical models (Wolery, 1992; Wolery and Daveler, 1992) and CHIM-XPT (Reed et al. 2016) to constrain the effects of scrubbing through hydrothermal systems of varying maturity, T, and water chemistries. Sulfur outputs were compared to high- and low-T fumarole and plume compositions to evaluate the relative importance of different volcanic processes.

2 Geological setting

2.1 Whakaari

Whakaari is Aotearoa New Zealand's most active volcano (see review by Kilgour et al., 2021), located ~50 km offshore of the North Island in the Bay of Plenty (Figure 1a). It is at the north end of the Taupō Volcanic Zone, which is a rifted arc caused by oblique, westward subduction of the Pacific plate under the Australian plate (Cole, 1990; Wallace et al., 2004). The volcano sits on continental crust and is mostly composed of andesitic to dacitic magmas, with occasional high-Mg andesites (e.g., Cole et al., 2000). The magmas are relatively H_2O-poor, with <1.5 wt% H_2O recorded in melt inclusions and from plagioclase hygrometry (Wardell et al., 2001; Rapien et al., 2003; Esposito et al., 2014; Mandon et al., 2021; Kilgour et al., 2021). Degassing is primarily passive (i.e., non-eruptive) and occurs through vents within the main crater, distributed fumaroles on the broader crater floor, and diffuse degassing (e.g., Wardell et al., 2001). There is an active hydrothermal system consisting of mixtures of seawater, brine, and/or meteoric water and the main crater periodically infills with a lake (e.g., Christenson et al., 2017; Kilgour et al., 2021; Giggenbach et al., 2003). Hydrothermal fluids may circulate to a depth of ~1 km, whereas a two-phase (gas + fluid) system occurs at shallower levels (Jolly et al., 2017). Permeabilities throughout the hydrothermal system vary widely depending on localized fracturing, dissolution, or mineral precipitation (Heap et al., 2017). Between 2005–2015, 127 ± 71 t/d S was emitted during passive degassing using a combination of space-based and ground-based measurements (Fischer et al., 2019). The GeoNet program regularly monitors the volcano which, prior to the 2019 eruption, included on-the-ground measurements of fumarole temperatures (T) and compositions; crater lake height and T; and ground deformation. Since 2019, on-the-ground monitoring has not been undertaken and real-time seismo-acoustic monitoring has degraded gradually. At the time of writing, (as of October 2023) all on-the-ground monitoring is no longer operational. Airborne measurements of SO_2, H_2S, and CO_2 flux from the plume, plus observation flights are continuing. All monitoring data for Whakaari are freely available from the GeoNet website (https://www.geonet.org.nz/).
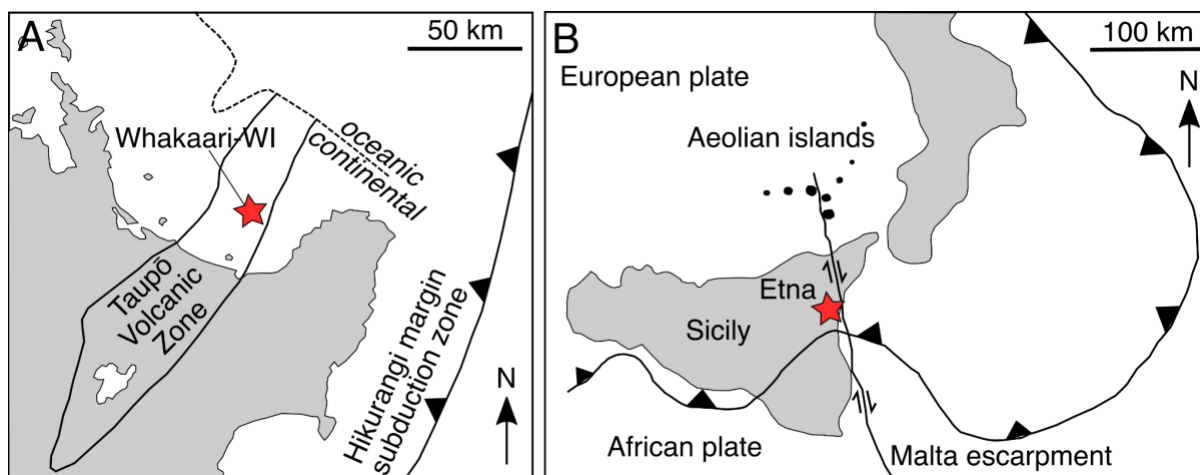
3

Figure 1 Location and simplified tectonic setting of the two volcanoes chosen for this study: **(a)** Whakaari/White Island (WI), Aotearoa New Zealand, and **(b)** Etna, Italy. Modified from Cole et al. (2000) and Kahl et al. (2015), respectively.

2.2 Etna

Etna is one of the most active basaltic volcanoes in the world and is located on the island of Sicily, Italy (Figure 1b). It occurs at the intersection between the Aeolian arc (related to the collision of the African and European plates) and the Malta escarpment (e.g., Barberi et al., 1974). The magma composition is intermediate between ocean island and island arc basalts (e.g., Schiano et al., 2001). The eruption style at Etna is highly varied (effusive lava flows to explosive Plinian eruptions), and erupted magmas are often volatile-rich (e.g., Coltelli et al., 1998; Metrich et al., 2004; Burton et al., 2005). The volcano is persistently degassing from multiple summit vents through many fumaroles and extensive diffuse flank degassing (e.g., Aiuppa et al., 2006; Allard et al., 2006; Hernández et al., 2015). Etna emitted 1052 ± 532 t/d S both passively (using data between 2005–2015) and during eruptions (using data between 2005–2017) using space and ground-based measurements (Fischer et al., 2019). The extent of the hydrothermal system present at Etna is smaller than that at Whakaari and is characterized by small-scale, shallow pockets of mostly meteoric hydrothermal fluids near active vents, as well as the likely presence of deeper hydrothermal brines (Brusca et al., 2001; Behnke et al., 2008). Based on thermochemical modeling, Liotta et al. (2010) report that the conversion of SO_2 into H_2S happens rapidly as exsolved magmatic gas cools from 1150 to 400 °C, resulting in molar SO_2/H_2S between 1 and 5. Partial dissolution of SO_2 and H_2S occurs as gases intersect unsealed fractures filled with near boiling water of an uncertain, but likely meteoric, origin at high-P (>50 bars) and high-T (>260 °C). At shallower P, the interactions between hydrothermal fluids and ascending gases occur too rapidly for efficient scrubbing (i.e., dissolution into H_2O) of SO_2 (Giammanco et al., 1998; Liotta et al., 2010).

3 Methods

We model the flux and composition of volatile components from when they are dissolved in the initial melt to emission at the surface including the effects of crystallization, degassing, and water-gas-rock reactions (Figure 2). By comparing the modeled and measured volatile flux and composition at different stages within the volcanic system, we can evaluate which processes are occurring and their relative importance. Compositional input data to the various models, as well as measured gas flux and fumarole and plume compositions for Whakaari and Etna are given in the Supplementary Material.
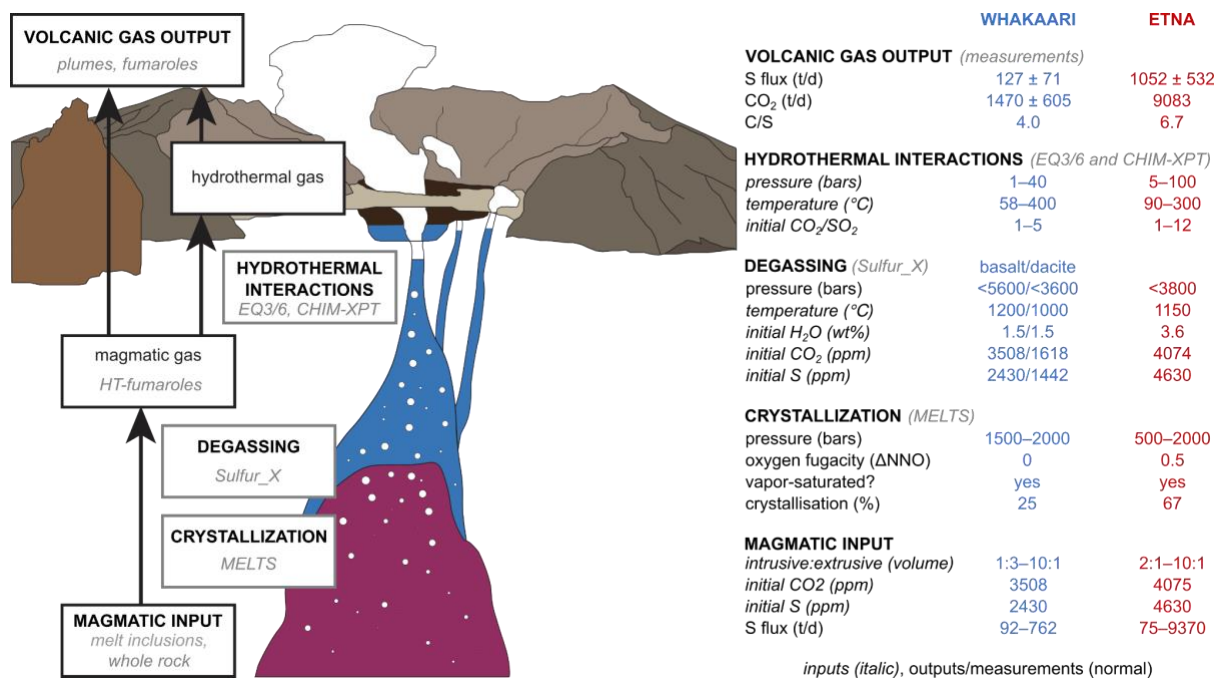
	WHAKAARI	ETNA
VOLCANIC GAS OUTPUT *(measurements)*		
S flux (t/d)	127 ± 71	1052 ± 532
CO_2 (t/d)	1470 ± 605	9083
C/S	4.0	6.7
HYDROTHERMAL INTERACTIONS *(EQ3/6 and CHIM-XPT)*		
pressure (bars)	1–40	5–100
temperature (°C)	58–400	90–300
initial CO_2/SO_2	1–5	1–12
DEGASSING *(Sulfur_X)*	basalt/dacite	
pressure (bars)	<5600/<3600	<3800
temperature (°C)	1200/1000	1150
initial H_2O (wt%)	1.5/1.5	3.6
initial CO_2 (ppm)	3508/1618	4074
initial S (ppm)	2430/1442	4630
CRYSTALLIZATION *(MELTS)*		
pressure (bars)	1500–2000	500–2000
oxygen fugacity (ΔNNO)	0	0.5
vapor-saturated?	yes	yes
crystallisation (%)	25	67
MAGMATIC INPUT		
intrusive:extrusive (volume)	1:3–10:1	2:1–10:1
initial CO2 (ppm)	3508	4075
initial S (ppm)	2430	4630
S flux (t/d)	92–762	75–9370

inputs (italic), outputs/measurements (normal)

Figure 2. *(left)* Schematic illustration showing our approach to modeling sulfur in the magmatic-hydrothermal systems (in purple and blue, respectively) of both Whakaari and Etna (illustration: Whakaari). Reservoirs of sulfur are shown in black outlined boxes, with observables of these reservoirs shown in *gray italics*. Processes affecting sulfur as it moves between reservoirs are shown in boxes outlined in gray, where the program used to model this process is shown in *gray italics*. *(right)* Table indicating the processes considered in our approach (**black bold**) including: programs used for modeling (*gray italics*), inputs used for the models (*italics*), outputs and best-fit solutions (normal), and measurements made at the volcanoes (normal) for Whakaari (left, blue) and Etna (right, red).

3.1 Magmatic input and crystallization

To quantify the sulfur inputs into the volcanic-hydrothermal systems at Whakaari and Etna, we assume that the only sulfur input is mantle-derived sulfur from the primary magma (i.e., there is no addition of crustal material). Crustal contamination is thought to be limited in both systems, and the true composition of any assimilant would be very difficult to determine (Cole et al., 2000; Heyworth et al., 2007; Corsaro and Pompilio, 2004). To calculate the sulfur input we require an estimate of: (1) the initial concentration of sulfur in primary magmas, and (2) the primary magma flux from the mantle.

The sulfur content of the mantle-derived parent melt is a function of the sulfur concentration in subduction-modified mantle, oxygen fugacity (f_{O2}) of the mantle source, and the extent of mantle melting (e.g., Ding & Dasgupta, 2018; Chowdhury & Dasgupta, 2019; Muth and Wallace, 2022). At low degrees of partial melting, if there is a residual sulfate and/or sulfide phase in the mantle after partial melting, then the sulfur content of the mantle-derived melt would be governed by the sulfur content at anhydrite or sulfide saturation. At higher degrees of partial melting, when sulfide and sulfate phases would likely have been exhausted, the sulfur content of the melt is governed by the amount of sulfide and/or sulfate phases initially present, and the sulfur concentration in the melt would become diluted as more melt is generated. As both volcanoes are in subduction zone settings, our estimate of initial sulfur content of the mantle is affected by uncertainty in the contribution from the subducting slab and the degree of partial melting. Therefore, our best estimate of the initial sulfur concentration

of the primary magma is the highest measured sulfur concentration from primitive melt inclusions. We compiled melt inclusion data from Whakaari (Rapien et al., 2003; Wardell et al., 2001; Esposito et al., 2014; Mandon et al., 2021; Kilgour et al., 2021) and Etna eruptions between 2001–2016 (Metrich et al., 2004; Spilliaert et al., 2006; Collins et al., 2009; Schiavi et al., 2015; Gennaro et al., 2019; Edwards & Pioli, 2019; Potter et al., 2019). Measured sulfur concentrations are as much as 2430 and 4630 ppm in Whakaari and Etna, respectively, and we use these values as the starting values for petrogenetic modeling (full dataset available in the Supplementary Material).

We constrain the parental magma flux into the system using estimates of the time period over which a certain volume of primary magma entered the system. Both time and volume are challenging to constrain. Estimating the volume of magma which enters the system requires knowledge of both the intruded and extruded magma volumes, where I:E is the ratio of intrusive to extrusive magma volumes.

The extruded magma volume (and flux) can be estimated from observed volumes of erupted magma over a known time interval. For Whakaari, we used the edifice volume as the extruded magma volume (78 km^3; Duncan 1970; Cole et al., 2000) and the total edifice age (10 to 21 kyrs; Rapien et al., 2003; Shane et al., 2006). We note that the edifice volume used here is likely a minimum considering syn/post-eruptive surface processes (e.g., deposition of material into the sea, edifice collapse and destruction) have likely removed an unknown volume of material from the current edifice over time. For Etna we used two different approaches: (1) total estimated eruptive volume during the lifetime of the volcano (350 km^3 over ~500 kyrs, Tanguy et al. 1997); and (2) directly calculated eruptive volumes during observed eruptions between 1970–2010 (Harris et al., 2011).

The intruded magma volume is more difficult to constrain due to lack of direct observations. A minimum estimate comes from the amount of crystallization of the primary magma required to produce the composition of erupted material calculated using MELTS modeling (Ghiorso & Sack 1995; Asimow & Ghiorso 1998). We assumed that the most primitive lavas were representative of the 'primary' magma compositions in both volcanic systems. A grid-search through a range of parameters (1300–700 °C T, relative f_{O2} (ΔNNO, where ΔNNO is log f_{O2} (melt) – log f_{O2} (Ni-NiO buffer)) of -3 to +3, 0–10 kbar P, and 0 wt% to H_2O-saturated conditions) during fractional crystallization was used to find a liquid line of descent that would best match measured whole rock compositions. The best match was evaluated using least-squares residuals to measured MgO, CaO, Al_2O_3, and SiO_2 in bulk rock samples, as these oxides are most sensitive to variations in crystallization conditions. MELTS continuously tracks the mass of residual melt during fractional crystallization, allowing us to correct for the mass of crystals removed from each system due to fractional crystallization, and by extension, to estimate the mass of parent (least evolved) magma contributing to the total sulfur budget for each system. Combining the observed extruded magma volume with the calculated intrusive to extrusive ratio (I:E) from MELTS modeling yields an estimate for the total volume of parental magma and the inferred volume of cumulate material left in the crust.

However, some magma intruded in the crust may not have contributed to erupted magma at the surface. Therefore, the maximum estimate of the primary magma flux (and therefore S flux) depends on the maximum I:E assumed. Excess SO_2 flux measurements at volcanoes (i.e., more SO_2 emitted than could be derived from the erupted magma) can be used to constrain I:E (e.g., Steffke et al., 2011). However, using empirically constrained I:E at Whakaari or Etna to estimate the S flux would lead to circular arguments. We therefore conducted a series of calculations for both systems using I:E up to 10:1 (these are reasonable ratios proposed for other systems; Steffke et al., 2011) to better quantify the effect of residual unerupted magma on estimated S flux.

As an alternative, we estimate SO_2 flux using the measured CO_2 flux and an estimate of the initial C/S ratio of the magma. This calculation assumes that the magma completely degasses CO_2 and that all CO_2 released from the magma reaches the surface. For CO_2 flux, we use the average of GeoNet data for Whakaari (1470 ± 605 t/d) and the value from Aiuppa et al. (2019) for Etna (9083 t/d). For the initial C/S ratio, we use the ratio of the highest measured S and CO_2 concentrations from our melt inclusion compilation from each volcano: 3508 ppm CO_2 and 2430 ppm S for Whakaari, and 4075 ppm CO_2 and 4630 ppm S for Etna (discussed in Section 3.3).

3.3 Degassing: Sulfur_X

We used Sulfur_X (Ding et al., 2023) to simulate degassing of typical Whakaari and Etna magmas as they ascend through the crust. We compare the observed gas compositions measured at fumaroles and plumes to the calculated compositions during the degassing paths. This approach provides insight on the pressure at which the gas may have separated from the magma; and whether the observed gas compositions emitted at the surface can be generated by degassing alone or if they require the influence of the hydrothermal system.

Sulfur_X predicts the equilibrium melt and vapor compositions for multi-volatile systems (CO_2, H_2O, SO_2, and H_2S) under closed-system degassing conditions. The solubility of CO_2 and H_2O in the melt is related to the fugacity of these species in the gas phase. Sulfur is modeled using two empirically-calibrated partition coefficients for mafic magmas between H_2S in the vapor and S^{2-} in the melt and SO_2 in the vapor and S^{6+} in the melt. For all our modeling, we turn crystallization off (i.e., there is a single melt composition during decompression) and we allow f_{O2} to vary during degassing. For the sulfur speciation in the melt we used the model of Muth & Wallace (2022), whilst for C-O-H solubility we used the model from VolatileCalc (Newman & Lowenstern, 2002) for the Whakaari basalt and Iacono-Marziano et al. (2012) for Whakaari dacite and Etna basalt. Due to the uncertainties in the sulfur partition coefficients in Sulfur_X, we typically do not consider outputs from $P \lesssim 20\text{--}30$ bars (Ding et al., 2023). We note that the compositional calibration for Sulfur_X does not extend to dacitic compositions, and therefore we interpret the results of the dacite models with caution.

For modeling Whakaari, we investigated two compositions (basalt and dacite) to simulate potential degassing scenarios from what are likely complexly configured magma storage zones beneath the volcano. Our initial conditions are based primarily on our melt inclusion data compilation. The model melt composition was the lowest SiO_2 melt composition (basalt) or average of melt inclusions with $SiO_2 > 60$ wt% (andesite-dacite). Temperature was based on thermometry from Kilgour et al. (2021): 1200 °C (basalt) and 1000 °C (dacite). We assumed 1.5 wt% H_2O for both the basalt and dacite based on hygrometry from Kilgour et al. (2021). Initial CO_2 used the highest (3508 ppm) and second highest (1618 ppm) values from melt inclusions for the basalt and dacite, respectively (Esposito et al., 2014). The sulfur content used the highest concentration from basaltic (2430 ppm) and andesite-dacite ($SiO_2 > 60$ wt%, 1442 ppm) melt inclusions. The f_{O2} is poorly constrained: we use ΔNNO=0 as stated in Kilgour et al. (2021) for basalt and dacite, which is consistent with our MELTS modeling presented in Section 4.2.

For modeling Etna, the melt composition chosen was the most primitive melt inclusion (lowest SiO_2) from the 2001–2003 eruptions at Etna (Gennaro et al., 2019) at 1150 °C and ΔNNO+0.5 (Gaborieau et al., 2020; consistent with MELTS modelling in Section 4.2). The initial volatile content is the highest from our melt inclusion data compilation: 3.6 wt%

H$_2$O, 4075 ppm CO$_2$ and 4630 ppm S. Full details of the inputs for these simulations are given in the Supplementary Material.

3.4 Hydrothermal interactions: EQ3/6 and CHIM-XPT

We use the EQ3/6 geochemical modeling software to investigate the effects of varying hydrothermal parameters (water chemistry, *T*, *P*) on surface emissions of CO$_2$, SO$_2$, and H$_2$S at Whakaari and Etna. We compare modeled and measured surface CO$_2$, SO$_2$, and H$_2$S emissions at each volcano to characterize whether magmatic gas titrated through hydrothermal fluids under different conditions can recreate the compositions of measured surface emissions. Our approach follows the work of Di Napoli et al. (2016) using the EQ3/6 geochemical modeling software within the Enabling Knowledge Integration (ENKI) (http://enki-portal.org/) server through the Jupyter Notebooks open-source web application. We use the jus.R60 thermodynamic database with a maximum *T* of 350 °C and *P* of 165.2 bars. An initial packet of bulk magmatic gas (compositions taken from high-*T* fumaroles) is titrated into, and allowed to equilibrate at different *T* and *P*, with a system consisting of bulk bedrock and various water compositions set to represent a hydrothermal system. The output composition of gas phase components is recorded after titration and equilibration with the water-rock system at the indicated *P* and *T* regime. All models were run in the 'relative rates' mode using the transition state theory rate law to model irreversible reactions between the minerals and waters (Wolery, 1992; Wolery and Daveler, 1992). Inputs into EQ3/6 are given in the Supplementary Material. Note that the EQ3/6 input did not allow for definition of H$_2$O (gas) as a titrant: therefore, our input magmatic gases are defined solely based on CO$_2$ and SO$_2$ molar ratios.

At Whakaari, we performed four to nine total runs for each water composition-*P-T* regime based on whether there was large variance between subsequent runs. To reflect changing hydrothermal conditions due to interaction with hydrothermal gases, each step within a run used the water output from the previous step and the same initial magmatic gas composition. The bulk rock composition used was the Whakaari central cone dacite from Cole et al. (2000). The initial magmatic gas packet was assumed to be the composition of high-*T* fumaroles with CO$_2$/SO$_2$ = 5 (Giggenbach et al., 1975) and was titrated through four different water compositions: brine (Christenson et al., 2017), seawater (McCollom, 2007), meteoric water (Berner and Berner, 2012; Hao et al., 2017), and lake water (Christenson et al., 2017).

For Etna, we performed five total model runs for each water composition-*P-T* regime, with each step using the water output from the previous step and the same initial magmatic gas composition. For the *T* and *P* of the Etna hydrothermal system, we used values from Giammanco et al. (1998). We define a magmatic gas input of CO$_2$/SO$_2$ = 12 based on a multigas measurement by Aiuppa et al. (2008), taken when CO$_2$ flux was highest during the pre-eruptive period (CO$_2$ = 19062 t/d, SO$_2$ = 1631 t/d, H$_2$O = 13257 t/d). The bulk rock composition used was K-trachybasalt (Giuffrida & Viccaro, 2017). Finally, we used an initial deep brine composition from sample 19 of Brusca et al. (2001) and a meteoric water composition from Berner and Berner (2012).

To characterize the effect water has on sulfur flux through hydrothermal systems, we used the program CHIM-XPT (formerly known as CHILLER; Reed et al. 2016). CHIM-XPT has the capability to compute reaction processes in water-rock-gas systems. Reaction processes can be calculated under changing composition, *P*, and *T*. CHIM-XPT modelling is restricted to *P* < 5000 bar and *T* < 600 °C. For our purpose, we titrated gas of a specific composition through water to see the output gas composition. This was done to test the effect of scrubbing on gases titrated through the hydrothermal system at Whakaari. Rock composition was not considered.

Input gas compositions came from high-T fumaroles (Giggenbach, 1987), which were used as a proxy for gases sourced from the underlying magma. We chose specific water geochemistry of samples collected from hot springs located in the crater (Giggenbach, 1987) as a best representative for the composition of the hydrothermal system. The models were run at 250 °C and 40 bars based on previous characterizations of Whakaari's hydrothermal system (e.g., Giggenbach, 1987, 2003). CHIM-XPT bases its calculations on 1 kg of water and outputs a water/gas ratio (w/g) based on the amount and type of gas that is input into the model. This output ratio can be scaled to larger volumes. We tested the evolution of a hydrothermal system by titrating increasing amounts of gas into the system and tracking changes in output gas composition. These observations can also be used to make predictions about gas composition and transfer related to the maturity of hydrothermal systems. High water/gas ratios (w/g) imply efficient gas scrubbing, typically associated with immature systems, which predictably alters gas compositions by removing most of the SO_2. Low w/g represents a mature system that is no longer able to efficiently scrub SO_2. In this context, a mature system with a low w/g implies the hydrothermal system is saturated with volatiles allowing SO_2 to pass through the hydrothermal system relatively unaffected, thus no longer causing a scrubbing effect. Inputs to CHIM-XPT are given in the Supplementary Material.

4 Results

4.1 Calculated magmatic input vs. surface emissions

At Whakaari, the best fit to whole-rock data using MELTS modeling is found under isobaric (1500–2000 bars) fractional crystallization at water-saturated conditions and a relative f_{O2} of $\Delta NNO=0$ (Figure 5a and b). The most evolved compositions were reproduced by MELTS after ~25% crystallization of the parent magma (I:E = 1:3). At Etna, the best fits are found with isobaric fractional crystallization under water-saturated conditions at ~500 and 2000 bar and slightly more oxidized conditions ($\Delta NNO+0.5$; Figure 5c and d). The most evolved compositions require more extensive crystallization (~67%) of the parent magma (I:E = 2:1). In both cases, these conditions closely match inferred conditions from other petrologic and geophysical methods (e.g., Whakaari: Cole et al. 2000, Etna: Cannata et al. 2018; Cashman & Edmonds, 2019).
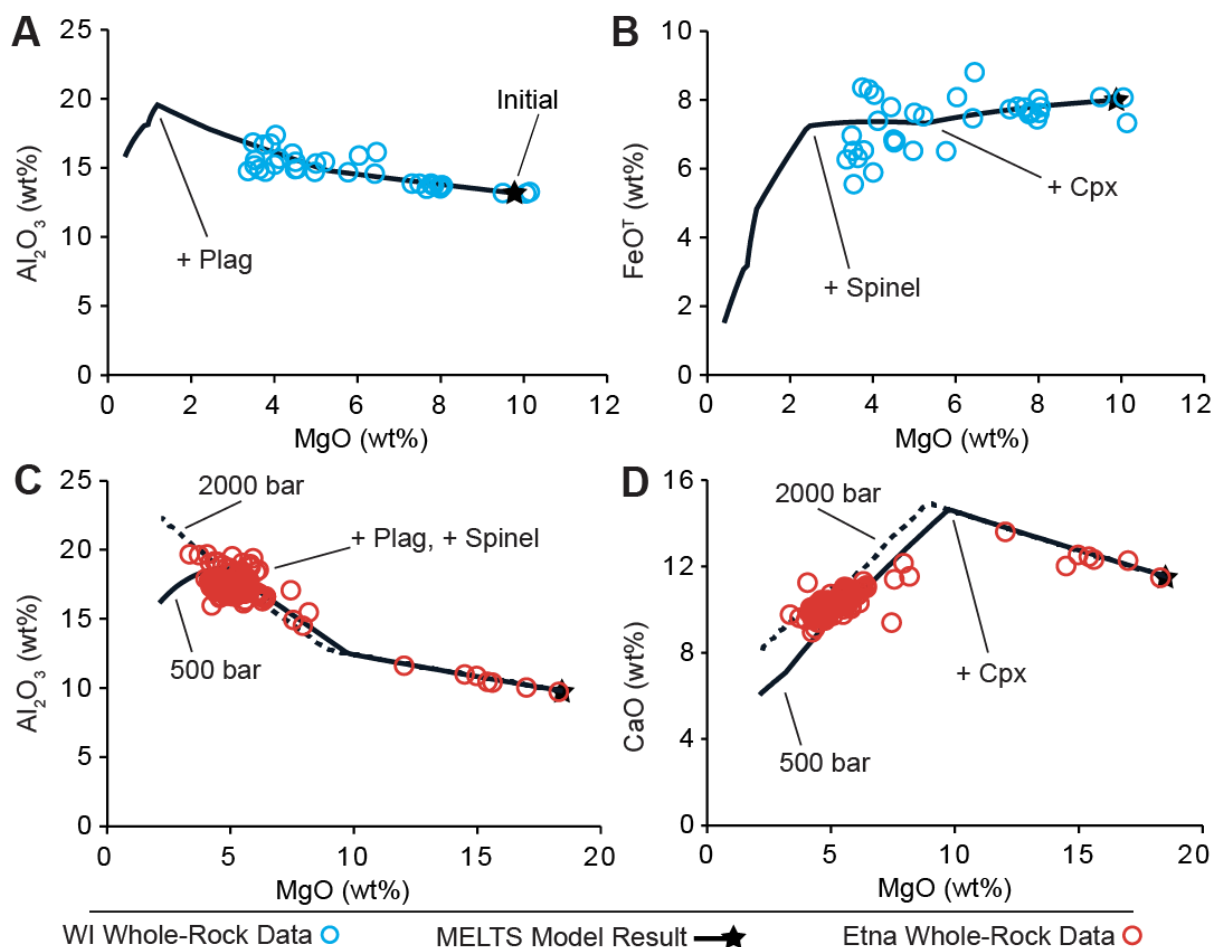
Figure 5 Results of MELTS modeling for **(a–b)** Whakaari (blue) with best fit parameters of isobaric fractional crystallization at 1500 bars, ΔNNO=0, and H_2O-saturated; and **(c–d)** Etna with best fit parameters of isobaric fractional crystallization at 500 bars (solid line) and 2000 bars (dashed line), ΔNNO+0.5, and H_2O-saturated. Whole rock data is shown by open symbols and MELTS modeling results by the black line, where the starting composition is shown by the black star. Data from Armienti et al. (1989); Tonarini et al. (1995); Cole et al. (2000); Corsaro et al. (2007); Kamenetsky et al. (2007); Heyworth et al. (2007); Viccaro and Cristofolini (2008); Correale et al. (2014); Viccaro et al. (2015); Gennaro et al. (2019); Di Renzo et al. (2019).

For Whakaari, our estimate for surface gas emissions is 92–762 t/d S (I:E = 1:3 to 10:1) and up to 1020 ± 420 t/d S (based on CO_2 flux), and the measured flux between 1983–2019 varies by two orders of magnitude (~3–900 t/d S; www.geonet.org.nz, Christensen et al., 2017), with an average of 127 ± 71 t/d S between 2005–2015 (Fischer et al., 2019) (Figure 6a). The wide range of estimated sulfur flux is due to uncertainty in the primary magma flux into the system (e.g., edifice age and volume, I:E). The minimum estimated flux based on intruded magma volume calculated using MELTS modeling is on the low end of measured flux values, but within error of the average flux between 2005–2015. The flux using an I:E = 1:1 is greater than the upper bound of 2005–2015 average.
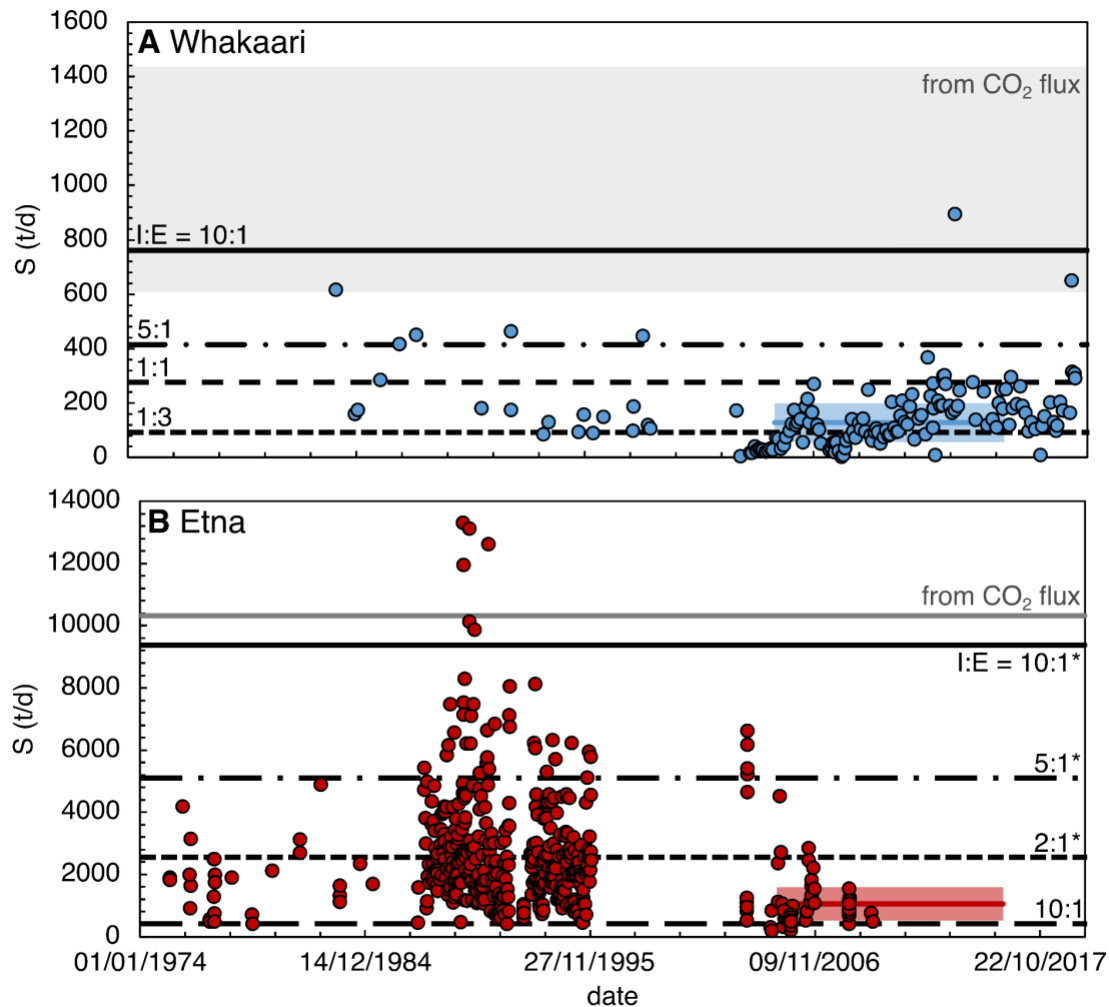
Figure 6 Sulfur flux (t/d S) for **(a)** Whakaari and **(b)** Etna. Circles are measured values (www.geonet.org.nz and Christensen et al. (2017) for Whakaari; Aiuppa et al. (2006, 2007 2008); Allard et al. (1991); La Spina et al. (2010); Salerno et al. (2009); Edner et al. (1994); Pugnaghi et al. (2006); Caltabiano et al. (1994); and Bruno et al. (1999) for Etna). The coloured box with the horizontal line (mean $\pm$ 1 standard deviation) represents the average output for 2005–2015 from Fischer et al. (2019). The horizontal black lines are calculated using different I:E ratios of 1:3 or 2:1 (dot - minimum value based on MELTS modeling), 1:1 (dash: Whakaari only), 5:1 (dot dash), and 10:1 (solid). Whakaari uses edifice volume and age to calculate eruption rates, whilst Etna uses observed eruption rates (indicated with a *; the black dashed line labeled 10:1 uses edifice volume and age for comparison). The gray region (Whakaari) and line (Etna) use measured CO_2 flux and initial C/S ratio of the magma.

For Etna, our estimate is 75–9370 t/d S using I:E = 2:1 to 10:1 and extruded volumes based on edifice volume to observed rates, and up to 10320 t/d S using CO_2 flux (Figure 6b; note the values obtained from edifice volume for I:E of 2:1 and 5:1 are not shown for clarity on the figure). The measured values range from 200 to 13300 t/d S (Aiuppa et al., 2006, 2007, 2008; Allard et al., 1991; La Spina et al., 2010; Salerno et al., 2009; Edner et al., 1994; Pugnaghi et al., 2006; Caltabiano et al., 1994; Bruno et al., 1999), with an average between 2005–2015 of 1052±532 t/d S (Fischer et al., 2019) (Figure 6b). Our minimum estimate (75 t/d S), derived from a long term erupted volume of ~350 km³, edifice age of ~500 kyrs (Tanguy et al., 1997), and I:E = 2:1, is approximately an order of magnitude lower than the average measured flux. The maximum estimate (10320 t/d S) uses measured CO_2 flux and initial C/S

ratio of the magma and is an order of magnitude larger than the recent average measured flux. The constraints on eruptive volume are more robust for the recent period (1970–2010) because of improved observations and monitoring of recent eruptions (Harris et al., 2011). Our modeling indicates that it is possible to balance the observed sulfur output at Etna if I:E < 2:1 for flux measurements since ~2003 and closer to 2:1 to 5:1 for older measurements.

4.4 Magmatic gas compositions

Figure 7 compares the outputs of Sulfur_X (Whakaari and Etna), EQ3/6 (Whakaari and Etna), and CHIM-XPT (Whakaari) with measured fumarole and plume compositions. At Whakaari, fumarole compositions are generally H_2O-rich, with higher T fumaroles being broadly richer in total sulfur (S_T) (Figure 7a). Both SO_2 and H_2S occur in the fumaroles (there is no systematic difference between high- and low-T fumaroles) but only SO_2 is present in the plume: molar SO_2/H_2S ratios range from 0 to 27 for fumaroles (Figure 7b). At Etna, fumarole compositions are poor in H_2O compared to Whakaari (Figure 7c). The SO_2/H_2S ratios for fumarole and plume compositions at Etna are highly variable, with SO_2/H_2S between 0.4 and 215 (Figure 7c).
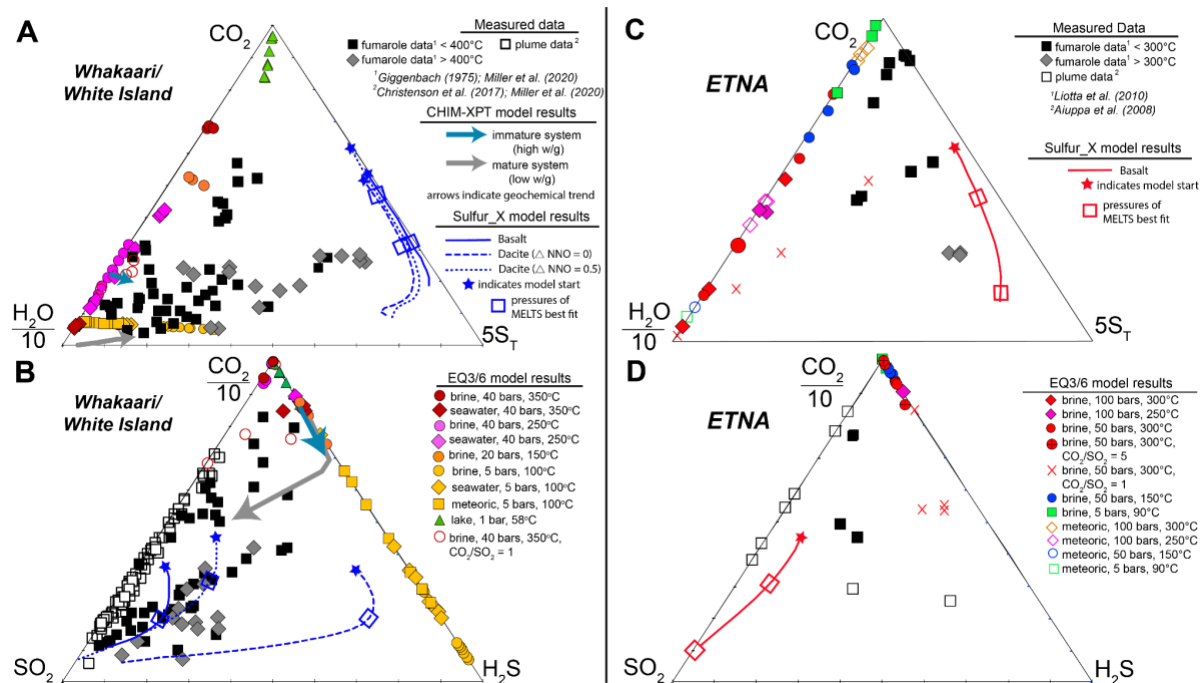

Figure 7 Gas composition for **(a–b)** Whakaari and **(c–d)** Etna plotted on ternary diagrams for **(a,c)** CO_2-H_2O-S_T and **(b,d)** CO_2-H_2S-SO_2. Model results are from Sulfur_X (blue (Whakaari) and red (Etna) curves; basalt = solid, dacite = dashed/dotted), EQ3/6 output gas emissions (colored symbols: initial magmatic $CO_2/SO_2 = 5$ for Whakaari and 12 for Etna unless otherwise noted), and CHIM-XPT (blue and gray arrows for Whakaari only). For comparison, plume (white squares) and fumaroles (black squares = high-T and grey diamonds = low-T) data are shown (Whakaari: Giggenbach, 1975; Christenson et al., 2017; Miller et al., 2020. Etna: Aiuppa et al., 2008; Liotta et al., 2010). High-T is >400 °C for Whakaari or >300 °C for Etna based on Giggenbach (1975) and Liotta et al. (2010), respectively.

4.5 Degassing: Sulfur_X

Results from Sulfur_X are shown using solid (basalt) and dashed (dacite) curves in Figure 7. All initial conditions predict decreasing CO_2 mole fraction in the vapor with decreasing P (curves start at the star in Figure 7a and c and move towards the H_2O-S_T edge with decreasing P). The degassing paths for basaltic compositions suggest the gas is SO_2-rich relative to H_2S, whereas the dacitic composition at Whakaari is more H_2S-rich (Figure 7b and d). Given the initial f_{O2} is uncertain for Whakaari magmas, we also modeled the dacitic melt composition using a slightly more oxidised f_{O2} (ΔNNO+0.5 vs. 0), shown as the dotted blue curves. This highlights that at the lower T of the dacite, the SO_2/H_2S ratio is highly dependent on modeled f_{O2} (e.g., Figure 2a in Ding et al, 2023).

For Whakaari, most of the fumarole data are more H_2O-rich than the gas compositions predicted by Sulfur_X (Figure 7a). Some of the plume and fumarole data have higher CO_2/SO_2 than the deepest results predicted by Sulfur_X, which may suggest a higher C/S ratio of the initial magma than used in our calculations. The plume data are notable in having $SO_2 \gg H_2S$. Some of the fumarole data have higher H_2S/SO_2 ratio than the basaltic and more oxidised dacitic degassing curves, but lower than the more reduced dacitic degassing curve (Figure 7b). Geologic evidence suggests that dacitic magma likely contributes to magmatic degassing at Whakaari. The more oxidised dacitic degassing path provides a better match to SO_2/H_2S > 1 values seen in high-T fumaroles, though we stress that initial f_{O2} is poorly constrained and Sulfur_X is not calibrated for dacitic compositions. Many lower-T fumarolic gases, however, cannot be explained by the magmatic degassing curves, indicating that magmatic degassing is not solely controlling the composition of volcanic gases at Whakaari, consistent with previous interpretations (Giggenbach, 1987).

For Etna the plume and fumarole gas compositions are broadly matched by the degassing curves, although some are more enriched in CO_2, H_2O, and H_2S than our degassing calculations (Figure 7c and d).

4.5 Hydrothermal interactions: EQ3/6

The EQ3/6 gas data in Figure 7 are the compositions of the magmatic gas outputs after titrating through, and equilibrating with, hydrothermal waters of various compositions at a range of T and P. The results plotted in Figure 7 across each T, P, and water chemistry regime represent the initial gas output, intermediate outputs, and the gas output of the final run (hence multiple occurrences of the same symbols in Figure 7) as the water chemistry evolves. At Whakaari, nearly all of the modeled gas outputs have compositions with low total sulfur (Figure 7a) and very high H_2S relative to SO_2 (Figure 7b) compared to the observed fumarole gas compositions. In an attempt to increase the SO_2/H_2S ratio of modeled surface gas emissions, we increased the amount of SO_2 in our initial magmatic gas compositions to CO_2/SO_2 = 1 and titrated it through brine at 350 °C and 40 bars (red outlined circles). This magmatic gas input with a higher concentration of SO_2 is the only modeled gas that plots closer to the region of measured gas compositions in Figure 7b but still has too low of an SO_2 concentration than most fumarole and plume measurements.

None of the modeled gas outputs from EQ3/6 intersect compositions of measured gas from Etna, as they are too S-poor (Figure 7c and d). We increased the amount of SO_2 in our initial magmatic gas compositions to CO_2/SO_2 = 5 (red circles with cross in Figure 7c, 8d) and CO_2/SO_2 = 1 (X symbols in Figure 7c and d) to test the effects of more SO_2-rich magmatic gas compositions entering the hydrothermal system. Only the models with CO_2/SO_2 = 1 have closer to the S_T of measured compositions (Figure 7c). Similar to Whakaari (Figure 7b), all EQ3/6 modeled output gases are too rich in H_2S relative to SO_2 (Figure 7d) when initial gas inputs are forced to equilibrate through hydrothermal water. The interactions modeled by EQ3/6 where
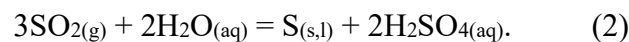
magmatic gas equilibrates with hydrothermal water does not reproduce the observed plume or fumarolic gas compositions at either Whakaari or Etna   .

4.6 Hydrothermal interactions: CHIM-XPT

CHIM-XPT produces output gas compositions that have experienced water-gas interactions that can ultimately be a reflection of hydrothermal system maturity. We only applied CHIM-XPT to Whakaari because of its well documented mature hydrothermal system (Giggenbach, 1987). We progressively input gas into Whakaari's hydrothermal system to test changes in output gas chemistry as the w/g ratio decreases (i.e., increasing amounts of gas input through a fixed mass of water). CHIM-XPT outputs the following gases and species for Whakaari: $H_2O_{(g)}$, $CO_{2(g)}$, $H_{2(g)}$, $H_2S_{(g)}$, $SO_{2(g)}$, $HF_{(g)}$, $HCl_{(g)}$, HSO_4^-, $SO_{2(aq)}$, $H_2S_{(aq)}$, $CO_{2(aq)}$, SO_4^{2-}, and Cl^-. Possible minerals precipitated are diaspore, anhydrite, pyrite, and native sulfur. Anhydrite and pyrite precipitate in minor proportions in an immature system, but sulfur was not precipitated in our models. Initially, output gas shows an increase in H_2S/SO_2 followed by a drastic decrease (Figure 8). An increase in H_2S/SO_2 is the direct result of hydrous interactions. SO_2 is consumed by hydrolysis reactions and produces H_2S (one form of scrubbing), thus initially increasing the H_2S/SO_2 ratio according to the following reactions (Giggenbach, 1987; Symonds et al., 2001):

$$4SO_{2(g)} + 4H_2O_{(aq)} = H_2S_{(aq)} + 3H_2SO_{4(aq)}, \qquad (1)$$

and,

$$3SO_{2(g)} + 2H_2O_{(aq)} = S_{(s,l)} + 2H_2SO_{4(aq)}. \qquad (2)$$

As more gas is titrated through the system, the SO_2 consumption decreases and scrubbing becomes less effective, causing the H_2S/SO_2 ratio of gas emissions to decrease (Figure 8). This decrease reflects maturation of a hydrothermal system that is no longer able to effectively scrub magmatic gases (Symonds et al. 2001).
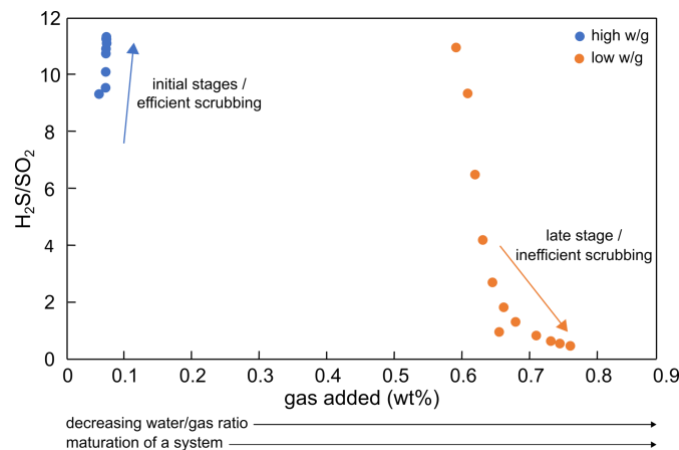

Figure 8 Results from CHIM-XPT modeling of Whakaari: changes in H_2S/SO_2 as gas is continually fed into the system. Initially there is a strong scrubbing effect that eventually diminishes as the water/gas ratio decreases.

Our model results show a comparison between these stages, representing the progression and evolution of a hydrothermal system as it experiences continual gas input and transitions from an immature (high w/g) to mature (low w/g) hydrothermal system with established gas pathways. We observe a significant change in H_2S/SO_2 for the initial stage where only a small amount of gas is titrated through the system. However, as more gas is incorporated into the system, the output H_2S/SO_2 ratio decreases because scrubbing becomes

less effective as the system evolves, and more gas is able to pass through without the effect of scrubbing.

On the ternaries in Figure 7a and b, the gas compositions related to the immature stage are shown by the blue arrow, and compositions related to the mature stage are shown by the gray arrow. Significant sulfur scrubbing occurs at the start of the immature stage, such that the CO_2/S_T of the first gas produced is much higher than the initial gas added to the system. During the immature stage, CO_2/H_2S ratio decreases as shown by the blue region in Figure 7b because scrubbing becomes less efficient but is still significantly less S-rich than the initial gas input. The modeled gas outputs for this immature, high w/g system (blue arrow) do not overlap with any of the measured fumarole or plume data. For the mature stage (gray arrow in Figure 7b) we see the effects of scrubbing further decrease as the concentration of SO_2 in the gas output increases. The modeled gas outputs with the highest SO_2 concentrations result in the only overlap with measured fumarole and plume compositions. Similar to the EQ3/6 modeled outputs, most of the measured compositions are not recreated by the CHIM-XPT models (Figure 7a and b).

5 Discussion

5.1 The effect of the hydrothermal system on surface gas emissions

To understand the effect of the hydrothermal system on the surface sulfur flux, we compare the gas compositions from our modeling results of magmatic degassing and water-gas-rock reactions to observed fumarole and plume compositions (Figure 7). These represent two end-member scenarios: magmatic degassing models (Sulfur_X) calculate changing gas composition from depth with no interaction with hydrothermal fluids, whereas water-gas± rock reactions (EQ3/6 and CHIM-XPT) force all of the emitted magmatic gas to interact with hydrothermal fluid. We also compare the pressure derived from the magmatic degassing models that match observed fumarole/plume compositions to the crystallization models using MELTS.

At Whakaari, the fumarole compositions mostly lie in between the results from magmatic degassing and hydrothermal interactions (Figure 7a and b). This suggests fumarole gases represent mixing of magmatic and hydrothermal gases or intermediate amounts of hydrothermal modification of magmatic gases. Mixing between magmatic gases and hydrothermal gases is well-known at Whakaari based on the variation in fumarole compositions (e.g., Giggenbach, 1987) and consistent with recent electrical resistivity studies at Whakaari that suggest the presence of a two-phase zone, likely comprised of gases in equilibrium with the hydrothermal system and higher T gases in equilibrium with the magma (Miller et al., 2020). The magmatic gas composition at the pressure of MELTs crystallization does not appear to be important. However, this uses a simplistic assumption that the gas separates from the melt at a single P. In reality degassing will occur throughout the magmatic system and gases will mix as they ascend (e.g., Iacovino, 2015). Additionally we only considered closed-system degassing because Sulfur_X is limited to modeling closed systems : open-system or a mixture of both open- and closed-system degassing are likely in magmatic systems.

CHIM-XPT model results also show a trend toward measured fumarole and plume compositions as the system evolves to lower w/g ratios (gray arrow in Figure 7b). This suggests that high-T fumaroles at Whakaari represent a mature hydrothermal system with a low w/g ratio and we refer to this magmatic gas pathway with a low water-gas interaction as a "dry gas

pathway". The formation of dry gas pathways is more likely to occur in volcanic systems like Whakaari that have prolonged periods of elevated activity (Symonds et al., 2001). This interpretation is consistent with Christensen et al. (2017), who proposed that large-scale deposition of hydrothermal minerals at Whakaari, such as elemental sulfur and anhydrite, can form a seal which creates a zone where a vapor-dominated phase can exist with low gas-water interaction. Our CHIM-XPT results did not precipitate elemental sulfur, which highlights that there are conditions in the hydrothermal system at Whakaari that are not well-reproduced by our modeling. A limitation of our EQ3/6 modeling is that the model did not reach the level of hydrothermal system maturity reached by the CHIM-XPT modeling due to using a higher w/g ratio. This is illustrated in Figure 7b, where our EQ3/6 gas outputs overlap the results from the "immature" stage of the hydrothermal system as indicated by CHIM-XPT modeling but do not follow a similar trend of decreasing H_2S/SO_2 characterizing the mature system.

In contrast, the plume compositions (only shown in the CO_2-SO_2-H_2S ternary, Figure 7b) at Whakaari do not lie between magmatic degassing and hydrothermal interaction compositions. They have a slightly higher SO_2/H_2S ratio than the magmatic degassing model results, away from hydrothermal gases. This suggests the plume gases do not react with, or mix with gases from, the hydrothermal system as much, though we note that reactions in the atmosphere can also increase the SO_2/H_2S ratio (although the kinetics of oxidation are thought to be sluggish; Aiuppa et al., 2005) .

At Etna, observed melt compositions can be reproduced by fractional crystallization at 500 to 2000 bars (Figure 5c and d). The magmatic gas composition at these depths is less CO_2-rich than the plume and fumarole compositions (Figure 7c and d). However, deeper-derived magmatic gases are more CO_2-rich and hence deeper gases (and gases from magmas with high initial C/S ratio) may be an important contribution to surface emissions (additionally, there are similar caveats about open- vs. closed-system degassing and mixing as discussed for Whakaari). The magmatic plumbing system at Etna is known to be complex, with multiple magma reservoirs present (e.g., Cashman & Edmonds, 2019). Therefore, gases from multiple depths are likely mixed to produce the gas composition at the surface.

Our EQ3/6 models produce gas outputs (after interaction with the hydrothermal system) with SO_2/H_2S values that are too low, whereas Sulfur_X models have SO_2/H_2S within the range of observed emissions (Figure 7d). Overall, gases modeled without hydrothermal interaction (through Sulfur_X) recreated the compositions of measured gases better than models from EQ3/6, although fumarolic gases do tend to contain more H_2O. Increasing the SO_2 concentration of our initial magmatic gas to $CO_2/SO_2 = 1$ still results in output gas emissions in EQ3/6 models that are too H_2S-rich ($SO_2/H_2S = 0.2$–0.4) when compared to measured fumarole emissions ($SO_2/H_2S = 1.5$–3.7). Therefore, our results suggest that shallow scrubbing processes are not occurring on a large-scale at Etna (Figure 7d), but our high w/g ratios may not be appropriate for this system. This supports Liotta et al. (2010), who found that water-gas interactions at Etna likely occur at P between 50–200 bars and T between 270–370°C based on thermochemical modeling (using the software HSC Chemistry) of cooling and condensing magmatic gases under a variety of T and P from depth to surface at Etna. At lower T and P, the interaction between fluids and ascending magmatic gases is too fast to allow for significant scrubbing of SO_2 at Etna (Giammanco et al., 1998; Liotta et al., 2010). Unfortunately, modeling of our data beyond 300°C was not possible using EQ3/6, limiting our ability to model gas-water interactions at higher T. However, Sulfur_X could not model the full range of measured SO_2/H_2S values and H_2O-enrichment of fumarole and plume gases emitted at Etna, suggesting

that some extent of hydrothermal interaction must exist to produce lower SO_2/H_2S ratios than what results from magma degassing alone.

5.2 Sulfur inputs and outputs over long time-scales

Our modeling of Whaakari and Etna suggest that over long timescales (at least 10s of years), sulfur inputs from mantle-derived primary magma can balance sulfur outputs as gaseous emissions to the atmosphere with I:E 1:3 to 1:1 for Whakaari or 2:1 to 5:1 for Etna (Figures 2 and 6). If I:E is < 1:3 for Whakaari (which is less than the minimum required to produce the composition of material erupted at the surface), additional sources of sulfur apart from the mantle-derived primary magma would be required (e.g., shallow crustal assimilation). For I:E > 1:1 for Whakaari or 5:1 for Etna, the sulfur output to the atmosphere is less than what is delivered by the long-term average mantle-derived primary magma input, which requires sulfur sequestration. We note that the I:E of 1:3 to 1:1 for Whakaari are relatively high given the low erupted volumes in recent history. Although gas interaction with hydrothermal water±rock does affect fumarolic gas compositions at Whakaari (and possibly to a small degree at Etna; see Section 5.1 for full discussion), the amount of sulfur sequestered by the hydrothermal systems of these volcanoes must be relatively small or relatively constant over geologic timescales, given the long-term emission data., However, the presence/absence and size of a hydrothermal system can significantly affect the release of sulfur to the atmosphere over short (years to decades) timescales (Giggenbach 1987). However, there are other processes that can sequester sulfur that we did not model, the most significant of which are discussed below.

Magmatic sulfide-saturation is thought to occur in the magmatic systems of both Whakaari and Etna (e.g., Spilliaert et al., 2006; Moretti et al., 2018; Mandon et al., 2020, 2021) but magmatic anhydrite has not been observed at either system. For Whakaari, ~2–20 t/d S may be sequestered as sulfides (Mandon et al., 2021). However, this S flux is smaller than the error in the average S flux between 2005-2015 (71 t/d) and hence is not an important flux to consider. At Etna, sulfide saturation is only thought to change melt sulfur concentrations temporarily (i.e., sulfides are often resorbed prior to eruption) and at a local spatial scale and therefore does not remove large amounts of sulfur from the system (e.g., Spilliaert et al., 2006; Gennaro et al., 2020). Hence, in both cases, removal of sulfur by magmatic sulfides is not likely to be important in overall sulfur fluxes.

High-*T* gas-solid reactions can also sequester sulfur in the sub-surface. Henley & Fischer (2021) found the potential for substantial sequestration of SO_2 through reactions with plagioclase and other Ca-bearing minerals, which produces anhydrite and reduced sulfur. Their modeling work showed that in andesitic systems with abundant Ca-bearing minerals this process could remove up to half of the mantle-derived sulfur from the high-*T* gas phase before it reaches the surface and thus increase fumarole C/S ratios (Henley & Fischer, 2021). If this process is important at Whakaari and/or Etna, it would suggest I:E > 5 for these systems. However, it is unclear for how long the sulfur is removed and how easily it would be remobilised.

At the surface, incomplete degassing of sulfur could also decrease the proportion of mantle-derived sulfur that is degassed at the surface during eruption. However, comparison of sulfur concentrations in whole rock data to initial melt inclusions suggest 92 % of sulfur is degassed at Whakaari during eruption (Mandon et al., 2020).

In summary, mantle-derived sulfur can explain the sulfur emissions from Whakaari if I:E = 1:3 to 1:1 and from Etna if I:E 2:1 to 5:1. If I:E is less than the lower bound, additional sulfur is required, which is inconsistent with additional constraints on these systems. If I:E is

greater than the upper bound, sulfur must be sequestered prior to surface emission. Magmatic sulfide formation and incomplete degassing are unlikely to be important processes for this, but high-T gas-solid reactions at both volcanoes and hydrothermal scrubbing at Whakaari could be.

5.3 Limitations

Our modeling of the volcanic systems at Whakaari and Etna are only as good as the data and models available. Ample bulk rock data are available for both systems, and the MELTS model is calibrated over a wide compositional range, hence the petrological modeling is likely robust. Although the sulfur content of the mantle feeding both volcanic systems is an important factor, the large uncertainties in the amount of sulfur being released from the slab at either system makes this difficult to constrain. Etna has abundant, Mg-rich olivine-hosted, basaltic melt inclusions, whereas Whakaari erupts predominantly more evolved material, which contains sparse olivine-hosted melt inclusions (e.g., Mandon et al., 2020; Kilgour et al., 2021), implying the initial sulfur content of Etna is more reliable than for Whakaari. However, the high S contents recorded in some olivine-hosted melt inclusions at Whakaari provides us with a minimum estimate for the initial S content of the primary magma.

A major limitation in our current approach is the suitability of available models for andesite-dacite degassing. Firstly, CO_2 solubility is highly melt composition dependent and its partitioning between melt and gas is important for general degassing trends (Brooker et al., 2001; Wallace, 2005; Papale et al., 2006; Moore, 2008). The uncertainty in CO_2 solubility is especially problematic for Whakaari, which has a predominantly andesitic-dacitic composition, as there is limited experimental data available for similar compositions (e.g., review by Weiser et al., 2022) resulting in a lack of dacite solubility constants. Similarly, the empirical models for S partition coefficients in Sulfur_X are based on experiments for mafic compositions and may not be appropriate for andesitic-dacitic melts.

Both volcanic systems had sufficient observational data to enable hydrothermal modeling using CHIM-XPT and EQ3/6. However, the current T range of these models does limit their applicability to certain systems. This is especially true in the case of Etna where high-T water-gas interactions may play a larger role than we were able to model (Liotta et al., 2010). Extending the hydrothermal modeling approach to include high-T gas-rock interactions (although the longevity of this interaction is unknown; e.g., Henley & Fischer, 2021) would be a further improvement and constraint on these two volcanic systems. Unfortunately, it would be difficult to extend this modeling attempt to most volcanoes due to insufficient data. However, testing our modeling approach at other well characterized systems (e.g., Ruapehu, Aotearoa New Zealand; Stromboli, Italy; Masaya, Nicaragua; Kīlauea, Hawaii; Yellowstone, USA; and Campi Flegrei, Italy) would help to evaluate the robustness of our generalizations.

6 Conclusions

Overall, we find that long-term inputs of sulfur into the volcanic systems at Whakaari and Etna can be broadly balanced by sulfur outputs over geologic timescales. We used observational constraints on the magmatic systems as inputs in thermodynamic, degassing, and hydrothermal models and compares the results to measured gas compositions. Low intrusive to extrusive ratios (I:E) would require additional sulfur sources to the mantle, which is inconsistent with other data on these volcanoes. High I:E would require that substantial sulfur is sequestered rather than being degassed to the atmosphere, such as during high-T gas-solid reactions (magmatic sulfide formation, and incomplete degassing are unlikely to be important).

However, the hydrothermal system modulates the compositions of fumarolic gases at Whakaari. The extent of scrubbing is dependent on the chemistry and maturity of the hydrothermal system, where there is a strong relationship between scrubbing and the water/gas ratio of the hydrothermal system.

At Whakaari, emitted gases appear to be mixtures of magmatic and hydrothermal gases or variably hydrothermally-modified magmatic gases and some portion of magmatic gas is being emitted without interaction with hydrothermal water at high-T fumaroles. Similarly, two end-member scenarios were tested at Etna: forcing all of the magmatic gas to interact with hydrothermal water or having no interaction between gas and water. Measured fumarole and plume data show gases emitted from Etna mostly comprise deeply derived magmatic gas but the higher H_2O, suggests the need for some hydrothermal interaction to fully describe the range of measured gas compositions.

Data availability

All data collated from the literature and used for this study are included in supplementary, as are any results from the modeling described in the paper.

Acknowledgements

References

Aiuppa, A., Inguaggiato, S., McGonigle, A.J.S., O'dwyer, M., Oppenheimer, C., Padgett, M.J., Rouwet, D. and Valenza, M., 2005. H_2S fluxes from Mt. Etna, Stromboli, and Vulcano (Italy) and implications for the sulfur budget at volcanoes. Geochimica et Cosmochimica Acta, 69(7), pp.1861-1871.

Aiuppa, A., Federico, C., Giudice, G., Gurrieri, S., Liuzzo, M., Shinohara, H., Favara, R. and Valenza, M., 2006. Rates of carbon dioxide plume degassing from Mount Etna volcano. *Journal of Geophysical Research: Solid Earth*, *111*(B9).

Aiuppa, A., Moretti, R., Federico, C., Giudice, G., Gurrieri, S., Liuzzo, M., Papale, P., Shinohara, H. and Valenza, M., 2007. Forecasting Etna eruptions by real-time observation of volcanic gas composition. *Geology*, *35*(12), pp.1115-1118.

Aiuppa, A., Giudice, G., Gurrieri, S., Liuzzo, M., Burton, M., Caltabiano, T., McGonigle, A.J.S., Salerno, G., Shinohara, H. and Valenza, M., 2008. Total volatile flux from Mount Etna. *Geophysical Research Letters*, *35*(24).

Aiuppa, A., Fischer, T.P., Plank, T., Robidoux, P. and Di Napoli, R., 2017. Along-arc, inter-arc and arc-to-arc variations in volcanic gas CO_2/S_T ratios reveal dual source of carbon in arc volcanism. *Earth-Science Reviews*, *168*, pp.24-47.

Aiuppa, A., Fischer, T.P., Plank, T. and Bani, P., 2019. CO_2 flux emissions from the Earth's most actively degassing volcanoes, 2005–2015. *Scientific reports*, *9*(1), pp.1-17.

Allard, P., Carbonnelle, J., Dajlevic, D., Le Bronec, J., Morel, P., Robe, M.C., Maurenas, J.M., Faivre-Pierret, R., Martin, D., Sabroux, J.C. and Zettwoog, P., 1991. Eruptive and diffuse emissions of CO_2 from Mount Etna. *Nature*, *351*(6325), pp.387-391.

Allard, P., Behncke, B., D'Amico, S., Neri, M. and Gambino, S., 2006. Mount Etna 1993–2005: Anatomy of an evolving eruptive cycle. *Earth-Science Reviews*, *78*(1-2), pp.85-114.

Alt, J. C., Shanks III, W. C., & Jackson, M. C. (1993). Cycling of sulfur in subduction zones: The geochemistry of sulfur in the Mariana Island Arc and back-arc trough. *Earth and Planetary Science Letters*, *119*(4), 477-494.

Alt, J.C., 1995. Sulfur isotopic profile through the oceanic crust: Sulfur mobility and seawater-crustal sulfur exchange during hydrothermal alteration. *Geology*, *23*(7), pp.585-588.

Armienti, P., Innocenti, F., Petrini, R., Pompilio, M., and Villari, L., 1989, Petrology and Sr-Nd isotope geochemistry of recent lavas from Mt. Etna: bearing on the volcano feeding system: Journal of Volcanology and Geothermal Research, v. 39, p. 315–327, doi:10.1016/0377-0273(89)90095-4.

Asimow, P.D. and Ghiorso, M.S., 1998. Algorithmic modifications extending MELTS to calculate subsolidus phase relations. *American mineralogist*, *83*(9-10), pp.1127-1132.

Baker, D.R. and Moretti, R., 2011. Modeling the solubility of sulfur in magmas: a 50-year old geochemical challenge. *Reviews in Mineralogy and Geochemistry*, *73*(1), pp.167-213.

Barberi, F., Civetta, L., Gasparini, P., Innocenti, F., Scandone, R. and Villari, L., 1974. Evolution of a section of the Africa-Europe plate boundary: paleomagnetic and volcanological evidence from Sicily. *Earth and Planetary Science Letters*, *22*(2), pp.123-132.

Beaudry, P., Longpré, M. A., Economos, R., Wing, B. A., Bui, T. H., & Stix, J. (2018). Degassing-induced fractionation of multiple sulphur isotopes unveils post-Archaean recycled oceanic crust signal in hotspot lava. *Nature communications*, *9*(1), 1-12.

Behncke, B., Calvari, S., Giammanco, S., Neri, M. and Pinkerton, H., 2008. Pyroclastic density currents resulting from the interaction of basaltic magma with hydrothermally altered rock: an example from the 2006 summit eruptions of Mount Etna, Italy. *Bulletin of Volcanology*, *70*(10), pp.1249-1268.

Berner, E.K. and Berner, R.A., 2012. *Global environment: water, air, and geochemical cycles*. Princeton University Press.

Blank, J.G., Stolper, E.M. and Carroll, M.R., 1993. Solubilities of carbon dioxide and water in rhyolitic melt at 850 C and 750 bars. *Earth and Planetary Science Letters*, *119*(1-2), pp.27-36.

Brooker, R.A., Kohn, S.C., Holloway, J.R. and McMillan, P.F., 2001. Structural controls on the solubility of CO2 in silicate melts: part I: bulk solubility data. *Chemical Geology*, *174*(1-3), pp.225-239.

Bruno, N., Caltabiano, T. and Romano, R., 1999. SO2 emissions at Mt. Etna with particular reference to the period 1993–1995. *Bulletin of Volcanology*, *60*(6), pp.405-411.

Brusca, L., Aiuppa, A., D'Alessandro, W., Parello, F., Allard, P. and Michel, A., 2001. Geochemical mapping of magmatic gas–water–rock interactions in the aquifer of Mount Etna volcano. *Journal of Volcanology and Geothermal Research*, *108*(1-4), pp.199-218.

Burgisser, A., Alletti, M. and Scaillet, B., 2015. Simulating the behavior of volatiles belonging to the C–O–H–S system in silicate melts under magmatic conditions with the software D-Compress. *Computers & Geosciences*, *79*, pp.1-14.

Burton, M.R., Neri, M., Andronico, D., Branca, S., Caltabiano, T., Calvari, S., Corsaro, R.A., Del Carlo, P., Lanzafame, G., Lodato, L. and Miraglia, L., 2005. Etna 2004–2005: An archetype for geodynamically-controlled effusive eruptions. *Geophysical research letters*, *32*(9).

Caltabiano, T., Romano, R. and Budetta, G., 1994. SO2 flux measurements at Mount Etna (Sicily). *Journal of Geophysical Research: Atmospheres*, *99*(D6), pp.12809-12819.

Cannata, A., Di Grazia, G., Giuffrida, M., Gresta, S., Palano, M., Sciotto, M., Viccaro, M. and Zuccarello, F., 2018. Space-time evolution of magma storage and transfer at Mt. Etna Volcano (Italy): the 2015–2016 Reawakening of Voragine Crater. *Geochemistry, Geophysics, Geosystems*, *19*(2), pp.471-495.

Carn, S.A., Fioletov, V.E., McLinden, C.A., Li, C. and Krotkov, N.A., 2017. A decade of global volcanic SO 2 emissions measured from space. *Scientific reports*, *7*(1), pp.1-12.

Cashman, K.V. and Edmonds, M., 2019. Mafic glass compositions: a record of magma storage conditions, mixing and ascent. *Philosophical Transactions of the Royal Society A, 377(2139)*.

Chowdhury, P. and Dasgupta, R., 2019. Effect of sulfate on the basaltic liquidus and sulfur Concentration at Anhydrite Saturation (SCAS) of hydrous basalts–Implications for sulfur cycle in subduction zones. *Chemical Geology*, *522*, pp.162-174.

Christenson, B.W., White, S., Britten, K. and Scott, B.J., 2017. Hydrological evolution and chemical structure of a hyper-acidic spring-lake system on Whakaari/White Island, NZ. *Journal of Volcanology and Geothermal Research*, *346*, pp.180-211.

Cicconi, M.R., Le Losq, C., Moretti, R. and Neuville, D.R., 2020. Magmas are the largest repositories and carriers of earth's redox processes. *Elements: An International Magazine of Mineralogy, Geochemistry, and Petrology*, *16*(3), pp.173-178.

Clemente, B., Scaillet, B., and Pichavant, M., 2004. The solubility of sulphur in hydrous rhyolitic melts. *Journal of Petrology* 45(11), pp.2171-2196.

Cole, J.W., 1990. Structural control and origin of volcanism in the Taupo volcanic zone, New Zealand. *Bulletin of volcanology*, *52*(6), pp.445-459.

Cole, J.W., Thordarson, T. and Burt, R.M., 2000. Magma origin and evolution of White Island (Whakaari) volcano, Bay of plenty, New Zealand. *Journal of Petrology*, *41*(6), pp.867-895.

Collins, S. J., Pyle, D. M., & Maclennan, J. (2009). Melt inclusions track pre-eruption storage and dehydration of magmas at Etna. *Geology*, *37*(6), 571-574.

Coltelli, M., Del Carlo, P. and Vezzoli, L., 1998. Discovery of a Plinian basaltic eruption of Roman age at Etna volcano, Italy. *Geology*, *26*(12), pp.1095-1098.

Correale, A., Paonita, A., Martelli, M., Rizzo, A., Rotolo, S.G., Corsaro, R.A., and Di Renzo, V., 2014, A two-component mantle source feeding Mt. Etna magmatism: Insights from the geochemistry of primitive magmas: Lithos, v. 184–187, p. 243–258, doi:10.1016/j.lithos.2013.10.038.

Corsaro, R.A., Miraglia, L., and Pompilio, M., 2007, Petrologic evidence of a complex plumbing system feeding the July–August 2001 eruption of Mt. Etna, Sicily, Italy: Bulletin of Volcanology, v. 69, p. 401–421, doi:10.1007/s00445-006-0083-4.

Corsaro, Rosa Anna, and Massimo Pompilio. "Dynamics of magmas at Mount Etna." GEOPHYSICAL MONOGRAPH-AMERICAN GEOPHYSICAL UNION. 143 (2004): 91-110.

De Hoog, J.C.M., Taylor, B.E. and Van Bergen, M.J., 2001. Sulfur isotope systematics of basaltic lavas from Indonesia: implications for the sulfur cycle in subduction zones. *Earth and Planetary Science Letters*, *189*(3-4), pp.237-252.

de Moor, J.M., Fischer, T.P., Sharp, Z.D., King, P.L., Wilke, M., Botcharnikov, R.E., Cottrell, E., Zelenski, M., Marty, B., Klimm, K. and Rivard, C., 2013. Sulfur degassing at Erta Ale (Ethiopia) and Masaya (Nicaragua) volcanoes: Implications for degassing processes and oxygen fugacities of basaltic systems. *Geochemistry, Geophysics, Geosystems*, *14*(10), pp.4076-4108.

de Moor, J.M., Aiuppa, A., Avard, G., Wehrmann, H., Dunbar, N., Muller, C., Tamburello, G., Giudice, G., Liuzzo, M., Moretti, R. and Conde, V., 2016a. Turmoil at Turrialba Volcano (Costa Rica): Degassing and eruptive processes inferred from high-frequency gas monitoring. *Journal of Geophysical Research: Solid Earth*, *121*(8), pp.5761-5775.

de Moor, J.M., Aiuppa, A., Pacheco, J., Avard, G., Kern, C., Liuzzo, M., Martinez, M., Giudice, G. and Fischer, T.P., 2016b. Short-period volcanic gas precursors to phreatic eruptions: Insights from Poás Volcano, Costa Rica. *Earth and Planetary Science Letters*, *442*, pp.218-227.

de Moor, J.M., Stix, J., Avard, G., Muller, C., Corrales, E., Diaz, J.A., Alan, A., Brenes, J., Pacheco, J., Aiuppa, A. and Fischer, T.P., 2019. Insights on hydrothermal-magmatic interactions and eruptive processes at Poás Volcano (Costa Rica) from high-frequency gas monitoring and drone measurements. *Geophysical Research Letters*, *46*(3), pp.1293-1302.

Di Napoli, R., Aiuppa, A., Bergsson, B., Ilyinskaya, E., Pfeffer, M.A., Guðjónsdóttir, S.R. and Valenza, M., 2016. Reaction path models of magmatic gas scrubbing. *Chemical Geology*, *420*, pp.251-269.

Di Renzo, V., Corsaro, R.A., Miraglia, L., Pompilio, M., and Civetta, L., 2019, Long and short-term magma differentiation at Mt. Etna as revealed by Sr-Nd isotopes and geochemical data: Earth-Science Reviews, v. 190, p. 112–130, doi:10.1016/j.earscirev.2018.12.008.

Ding, S. and Dasgupta, R., 2018. Sulfur inventory of ocean island basalt source regions constrained by modeling the fate of sulfide during decompression melting of a heterogeneous mantle. *Journal of Petrology*, *59*(7), pp.1281-1308.

Ding S, Plank T, Wallace PJ, Rasmussen DJ. Sulfur_X: A model of sulfur degassing during magma ascent. Geochemistry, Geophysics, Geosystems. 2023 Apr;24(4):e2022GC010552.

Duncan, A.R. and Vucetich, C.G., 1970. Volcanic activity on White Island, bay of plenty, 1966–69: Part 2—tephra eruptions—stratigraphy and petrography. *New Zealand journal of geology and geophysics*, *13*(4), pp.969-979.

Edner, H., Ragnarson, P., Svanberg, S., Wallinder, E., Ferrara, R., Cioni, R., Raco, B. and Taddeucci, G., 1994. Total fluxes of sulfur dioxide from the Italian volcanoes Etna, Stromboli, and Vulcano measured by differential absorption lidar and passive differential optical absorption spectroscopy. *Journal of Geophysical Research: Atmospheres*, *99*(D9), pp.18827-18838.

Edwards, M.J. and Pioli, L., 2019. Magma and tephra characteristics for the 17–25 May 2016 Mt Etna eruption. Data in brief 22, 65-71.

Esposito, R., Hunter, J., Schiffbauer, J.D., Shimizu, N. and Bodnar, R.J., 2014. An assessment of the reliability of melt inclusions as recorders of the pre-eruptive volatile content of magmas. *American Mineralogist*, *99*(5-6), pp.976-998.

Fischer, T.P., Ramírez, C., Mora-Amador, R.A., Hilton, D.R., Barnes, J.D., Sharp, Z.D., Le Brun, M., de Moor, J.M., Barry, P.H., Füri, E. and Shaw, A.M., 2015. Temporal variations in fumarole gas chemistry at Poás volcano, Costa Rica. *Journal of Volcanology and Geothermal Research*, *294*, pp.56-70.

Fischer, T.P., Arellano, S., Carn, S., Aiuppa, A., Galle, B., Allard, P., Lopez, T., Shinohara, H., Kelly, P., Werner, C. and Cardellini, C., 2019. The emissions of CO 2 and other volatiles from the world's subaerial volcanoes. *Scientific reports*, *9*(1), pp.1-11.

Gaborieau, M., Laubier, M., Bolfan-Casanova, N., McCammon, C.A., Vantelon, D., Chumakov, A.I., Schiavi, F., Neuville, D.R. and Venugopal, S., 2020. Determination of Fe3+/ΣFe of olivine-hosted melt inclusions using Mössbauer and XANES spectroscopy. *Chemical Geology*, *547*, p.119646.

Gennaro, E., Iacono-Marziano, G., Paonita, A., Rotolo, S.G., Martel, C., Rizzo, A.L., Pichavant, M. and Liotta, M., 2019. Melt inclusions track melt evolution and degassing of Etnean magmas in the last 15 ka. *Lithos*, *324*, pp.716-732.

Gennaro, E., Paonita, A., Iacono-Marziano, G., Moussallam, Y., Pichavant, M., Peters, N. and Martel, C., 2020. Sulphur behaviour and redox conditions in etnean magmas during magma differentiation and degassing. *Journal of Petrology*.

Ghiorso, M.S. and Sack, R.O., 1995. Chemical mass transfer in magmatic processes IV. A revised and internally consistent thermodynamic model for the interpolation and extrapolation of liquid-solid equilibria in magmatic systems at elevated temperatures and pressures. *Contributions to Mineralogy and Petrology*, *119*(2), pp.197-212.

Ghiorso, M.S., Hirschmann, M.M., Reiners, P.W. and Kress, V.C., 2002. The pMELTS: A revision of MELTS for improved calculation of phase relations and major element partitioning related to partial melting of the mantle to 3 GPa. *Geochemistry, Geophysics, Geosystems, 3(5)*, pp.1-35.

Giammanco, S., Inguaggiato, S. and Valenza, M., 1998. Soil and fumarole gases of Mount Etna: geochemistry and relations with volcanic activity. *Journal of volcanology and geothermal research*, *81*(3-4), pp.297-310.

Giggenbach, W.F., 1975. Variations in the carbon, sulfur and chlorine contents of volcanic gas discharges from White Island, New Zealand. *Bulletin Volcanologique*, *39*(1), pp.15-27.

Giggenbach, W., 1982. The chemical and isotopic composition of gas discharges from New Zealand andesitic volcanoes. *Bulletin volcanologique*, *45*(3), pp.253-255.

Giggenbach, W.F., 1987. Redox processes governing the chemistry of fumarolic gas discharges from White Island, New Zealand. *Applied Geochemistry*, *2*(2), pp.143-161.

Giggenbach, W.F., Shinohara, H., Kusakabe, M. and Ohba, T., 2003. Formation of acid volcanic brines through interaction of magmatic gases, seawater, and rock within the White Island volcanic-hydrothermal system, New Zealand. *Special Publication-Society of Economic Geologists*, *10*, pp.19-40.

Giuffrida, M. and Viccaro, M., 2017. Three years (2011–2013) of eruptive activity at Mt. Etna: working modes and timescales of the modern volcano plumbing system from micro-analytical studies of crystals. *Earth-Science Reviews*, *171*, pp.289-322.

Goff, F., Janik, C.J., Delgado, H., Werner, C., Counce, D., Stimac, J.A., Siebe, C., Love, S.P., Williams, S.N., Fischer, T. and Johnson, L., 1998. Geochemical surveillance of magmatic volatiles at Popocatépetl volcano, Mexico. *Geological Society of America Bulletin*, *110*(6), pp.695-710.

Goff, F., Love, S.P., Warren, R.G., Counce, D., Obenholzner, J., Siebe, C. and Schmidt, S.C., 2001. Passive infrared remote sensing evidence for large, intermittent CO2 emissions at Popocatépetl volcano, Mexico. *Chemical Geology*, *177*(1-2), pp.133-156.

Goff, F. and McMurtry, G.M., 2000. Tritium and stable isotopes of magmatic waters. *Journal of Volcanology and Geothermal Research*, *97*(1-4), pp.347-396.

Hao, J., Sverjensky, D.A. and Hazen, R.M., 2017. A model for late Archean chemical weathering and world average river water. *Earth and Planetary Science Letters*, *457*, pp.191-203.

Harris, A., Steffke, A., Calvari, S. and Spampinato, L., 2011. Thirty years of satellite-derived lava discharge rates at Etna: Implications for steady volumetric output. *Journal of Geophysical Research: Solid Earth*, *116*(B8).

Heap, M.J., Kennedy, B.M., Farquharson, J.I., Ashworth, J., Mayer, K., Letham-Brake, M., Reuschle, T., Gilg, H.A., Scheu, B., Lavallee, Y. and Siratovich, P., 2017. A multidisciplinary approach to quantify the permeability of the Whakaari/White Island volcanic hydrothermal system (Taupo Volcanic Zone, New Zealand). *Journal of Volcanology and Geothermal Research*, *332*, pp.88-108.

Henley, R.W. and Fischer, T.P., 2021. Sulfur sequestration and redox equilibria in volcanic gases. *Journal of Volcanology and Geothermal Research*, *414*, p.107181.

Heyworth, Z., Turner, S., Schaefer, B., Wood, B., George, R., Berlo, K., Cunningham, H., Price, R., Cook, C., and Gamble, J., 2007, 238U–230Th–226Ra–210Pb constraints on the genesis of high-Mg andesites at White Island, New Zealand: Chemical Geology, v. 243, p. 105–121, doi:10.1016/j.chemgeo.2007.05.012.

Holland, T., and Roger, P., 1991. "A compensated-Redlich-Kwong (CORK) equation for volumes and fugacities of CO_2 and H_2O in the range 1 bar to 50 kbar and 100–1600 °C." *Contributions to Mineralogy and Petrology, 109*(2), pp.265-273.

Hutchison, W., Finch, A.A. and Boyce, A.J., 2020. The sulfur isotope evolution of magmatic-hydrothermal fluids: insights into ore-forming processes. *Geochimica et Cosmochimica Acta*, *288*, pp.176-198.

Iacono-Marziano, G., Morizet, Y., Le Trong, E. and Gaillard, F., 2012. New experimental data and semi-empirical parameterization of H2O–CO2 solubility in mafic melts. Geochimica et Cosmochimica Acta, 97, pp.1-23.

Jolly, A.D., Lokmer, I., Thun, J., Salichon, J., Fry, B. and Chardot, L., 2017. Insights into fluid transport mechanisms at White Island from analysis of coupled very long-period (VLP), long-period (LP) and high-frequency (HF) earthquakes. *Journal of Volcanology and Geothermal Research*, *343*, pp.75-94.

Kamenetsky, V.S., Pompilio, M., Métrich, N., Sobolev, A.V., Kuzmin, D.V., and Thomas, R., 2007, Arrival of extremely volatile-rich high-Mg magmas changes explosivity of Mount Etna: Geology, v. 35, p. 255–258, doi:10.1130/G23163A.1.

Kagoshima, T., Sano, Y., Takahata, N., Maruoka, T., Fischer, T.P. and Hattori, K., 2015. Sulphur geodynamic cycle. *Scientific Reports*, *5*(1), pp.1-6.

Kilgour, G., Kennedy, B., Scott, B., Christenson, B., Jolly, A., Asher, A., Rosenberg, M. and Saunders, K., 2021. Whakaari/White Island: a review of New Zealand's most active volcano. *New Zealand Journal of Geology and Geophysics*, *64*.

Kilgour GN, Moune S, Christenson BW, Della Pasqua F., 2021. Insights into the 1976–2000 eruption episode of Whakaari/White Island, New Zealand: an eruption fuelled by repeated mafic recharge. *Bulletin of Volcanology, 83*.

La Spina, A., Burton, M. and Salerno, G.G., 2010. Unravelling the processes controlling gas emissions from the central and northeast craters of Mt. Etna. *Journal of Volcanology and Geothermal Research*, 198(3-4), pp.368-376.

Labidi, J., Cartigny, P., Birck, J.L., Assayag, N. and Bourrand, J.J., 2012. Determination of multiple sulfur isotopes in glasses: A reappraisal of the MORB δ34S. *Chemical Geology*, *334*, pp.189-198.

Labidi, J., & Cartigny, P. (2016). Negligible sulfur isotope fractionation during partial melting: Evidence from Garrett transform fault basalts, implications for the late-veneer and the hadean matte. *Earth and Planetary Science Letters*, *451*, 196-207.

Lee, C.T.A., Erdman, M., Yang, W., Ingram, L., Chin, E.J. and DePaolo, D.J., 2018. Sulfur isotopic compositions of deep arc cumulates. *Earth and Planetary Science Letters*, *500*, pp.76-85.

Li, J.L., Schwarzenbach, E.M., John, T., Ague, J.J., Huang, F., Gao, J., Klemd, R., Whitehouse, M.J. and Wang, X.S., 2020. Uncovering and quantifying the subduction zone sulfur cycle from the slab perspective. *Nature communications*, *11*(1), pp.1-12.

Liotta, M., Paonita, A., Caracausi, A., Martelli, M., Rizzo, A. and Favara, R., 2010. Hydrothermal processes governing the geochemistry of the crater fumaroles at Mount Etna volcano (Italy). *Chemical Geology*, *278*(1-2), pp.92-104.

Liotta, M., Rizzo, A., Paonita, A., Caracausi, A. and Martelli, M., 2012. Sulfur isotopic compositions of fumarolic and plume gases at Mount Etna (Italy) and inferences on their magmatic source. *Geochemistry, Geophysics, Geosystems*, *13*(5).

Lopez, T., Aguilera, F., Tassi, F., De Moor, J.M., Bobrowski, N., Aiuppa, A., Tamburello, G., Rizzo, A.L., Liuzzo, M., Viveiros, F. and Cardellini, C., 2018. New insights into the magmatic-hydrothermal system and volatile budget of Lastarria volcano, Chile: Integrated results from the 2014 IAVCEI CCVG 12th Volcanic Gas Workshop. *Geosphere*, *14*(3), pp.983-1007.

Mandeville, C.W., Sasaki, A., Saito, G., Faure, K., King, R. and Hauri, E., 1998. Open-system degassing of sulfur from Krakatau 1883 magma. *Earth and Planetary Science Letters*, *160*(3-4), pp.709-722.

Mandeville, C.W., Webster, J.D., Tappen, C., Taylor, B.E., Timbal, A., Sasaki, A., Hauri, E. and Bacon, C.R., 2009. Stable isotope and petrologic evidence for open-system degassing during the climactic and pre-climactic eruptions of Mt. Mazama, Crater Lake, Oregon. *Geochimica et Cosmochimica Acta*, *73*(10), pp.2978-3012.

Mandon, C.L., Seward, T.M. and Christenson, B.W., 2020. Volatile transport of metals and the Cu budget of the active White Island magmatic-hydrothermal system, New Zealand. *Journal of Volcanology and Geothermal Research*, *398*, p.106905.

Mandon, C.L., Christenson, B.W., Seward T.M., Schipper, C.I., 2021. Magma mixing, degassing and late sulfide saturation: Insights into the 1976–2000 eruptive sequence at White Island, New Zealand. Journal of Volcanology and Geothermal Research, *417*, 107299.

Marini, L., Moretti, R. and Accornero, M., 2011. Sulfur isotopes in magmatic-hydrothermal systems, melts, and magmas. *Reviews in Mineralogy and Geochemistry*, *73*(1), pp.423-492.

McCollom, T.M., 2007. Geochemical constraints on sources of metabolic energy for chemolithoautotrophy in ultramafic-hosted deep-sea hydrothermal systems. *Astrobiology*, *7*(6), pp.933-950.

Métrich, N., Allard, P., Spilliaert, N., Andronico, D. and Burton, M., 2004. 2001 flank eruption of the alkali-and volatile-rich primitive basalt responsible for Mount Etna's evolution in the last three decades. *Earth and Planetary Science Letters*, *228*(1-2), pp.1-17.

Miller, C.A., Christenson, B.W., Byrdina, S., Vandemeulebrouck, J., Brakenrig, T., Britten, K., Shanks, J. and Epstein, G., 2020. Snapshot of a magmatic/hydrothermal system from electrical resistivity tomography and fumarolic composition, Whakaari/White Island, New Zealand. *Journal of Volcanology and Geothermal Research*, *400*, p.106909.

Moore, G., 2008. Interpreting H2O and CO2 contents in melt inclusions: constraints from solubility experiments and modeling. *Reviews in Mineralogy and Geochemistry*, *69*(1), pp.333-362.

Moore, L.R., Gazel, E., Tuohy, R., Lloyd, A.S., Esposito, R., Steele-MacInnis, M., Hauri, E.H., Wallace, P.J., Plank, T. and Bodnar, R.J., 2015. Bubbles matter: An assessment of the contribution of vapor bubbles to melt inclusion volatile budgets. *American Mineralogist*, *100*(4), pp.806-823.

Moretti, R., Métrich, N., Arienzo, I., Di Renzo, V., Aiuppa, A. and Allard, P., 2018. Degassing vs. eruptive styles at Mt. Etna volcano (Sicily, Italy). Part I: Volatile stocking, gas fluxing, and the shift from low-energy to highly explosive basaltic eruptions. *Chemical Geology*, *482*, pp.1-17.

Moretti, R. and Stefánsson, A., 2020. Volcanic and geothermal redox engines. *Elements: An International Magazine of Mineralogy, Geochemistry, and Petrology*, *16*(3), pp.179-184.

Muth, M.J., Wallace, P.J. (2022) Sulfur recycling in subduction zones and the oxygen fugacity of mafic arc magmas. Earth and Planetary Science Letters, 599, doi.org/10.1016/j.epsl.2022.117836.

Newman, S. and Lowenstern, J.B., 2002. VolatileCalc: a silicate melt–H2O–CO2 solution model written in Visual Basic for excel. Computers & Geosciences, 28(5), pp.597-604.

Ohmoto, H., 1972. Systematics of sulfur and carbon isotopes in hydrothermal ore deposits. *Economic Geology*, *67*(5), pp.551-578.

Ohmoto, H. and Kerrick, D.M., 1977. Devatilization equilibria in graphitic systems. American Journal of Science, 277(8), pp.1013-1044.

Papale, P., Moretti, R. and Barbato, D., 2006. The compositional dependence of the saturation surface of H2O+ CO2 fluids in silicate melts. *Chemical Geology*, *229*(1-3), pp.78-95.

Patanè, D., Aiuppa, A., Aloisi, M., Behncke, B., Cannata, A., Coltelli, M., Di Grazia, G., Gambino, S., Gurrieri, S., Mattia, M. and Salerno, G., 2013. Insights into magma and fluid transfer at Mount Etna by a multiparametric approach: A model of the events leading to the 2011 eruptive cycle. *Journal of Geophysical Research: Solid Earth*, *118*(7), pp.3519-3539.

Potter, N.J., Carey, R.J., Andronico, D. and Costantini, L., 2019. Eruption dynamics of the 23 February 2013 event at Mt. Etna. Journal of Volcanology and Geothermal Research, 384, pp.241-250.

Pugnaghi, S., Gangale, G., Corradini, S. and Buongiorno, M.F., 2006. Mt. Etna sulfur dioxide flux monitoring using ASTER-TIR data and atmospheric observations. Journal of Volcanology and Geothermal Research, 152(1-2), pp.74-90.

Rapien, M.H., Bodnar, R.J., Simmons, S.F., Szabo, C.S., Wood, C.P. and Sutton, S.R., 2003. Melt inclusion study of the embryonic porphyry copper system at White Island, New Zealand. *Special Publication-Society of Economic Geologists*, *10*, pp.41-60.

Reed, M.H., Spycher, N.F. and Palandri, J., 2016. Users Guide for CHIM-XPT: A Program for Computing Reaction Processes in Aqueous-Mineral-Gas Systems and MINTAB Guide, Version 2.50. *Eugene, OR: University of Oregon*.

Richet, P., Bottinga, Y. and Javoy, M., 1977. A review of hydrogen, carbon, nitrogen, oxygen, sulphur, and chlorine stable isotope fractionation among gaseous molecules. *Annual Review of Earth and Planetary Sciences*, *5*(1), pp.65-110.

Robinson, B.W., 1987. Sulphur and sulphate-oxygen isotopes in New Zealand geothermal systems and volcanic discharges. In *Studies on sulphur isotope variations in nature*.

Salerno, G.G., Burton, M.R., Oppenheimer, C., Caltabiano, T., Randazzo, D., Bruno, N. and Longo, V., 2009. Three-years of SO2 flux measurements of Mt. Etna using an automated UV scanner array: Comparison with conventional traverses and uncertainties in flux retrieval. *Journal of Volcanology and Geothermal Research*, *183*(1-2), pp.76-83.

Schiano, P., Clocchiatti, R., Ottolini, L. and Busa, T., 2001. Transition of Mount Etna lavas from a mantle-plume to an island-arc magmatic source. *Nature*, *412*(6850), pp.900-904.

Schiavi, F., Rosciglione, A., Kitagawa, H., Kobayashi, K., Nakamura, E., Nuccio, P.M., Ottolini, L., Paonita, A. and Vannucci, R., 2015. Geochemical heterogeneities in magma beneath Mount Etna recorded by 2001–2006 melt inclusions. *Geochemistry, Geophysics, Geosystems*, *16*(7), pp.2109-2126.

Shane, P., Sikes, E.L. and Guilderson, T.P., 2006. Tephra beds in deep-sea cores off northern New Zealand: implications for the history of Taupo Volcanic Zone, Mayor Island and White Island volcanoes. *Journal of Volcanology and Geothermal Research*, *154*(3-4), pp.276-290.

Shaw, H.R., 1985. Links between magma-tectonic rate balances, plutonism, and volcanism. *Journal of Geophysical Research: Solid Earth*, *90*(B13), pp.11275-11288.

Shi, P. and Saxena, S.K., 1992. Thermodynamic modelling of the CHOS fluid system. *American Mineralogist*, *77*(9-10), pp.1038-1049.

Shinohara, H., Aiuppa, A., Giudice, G., Gurrieri, S. and Liuzzo, M., 2008. Variation of H2O/CO2 and CO2/SO2 ratios of volcanic gases discharged by continuous degassing of Mount Etna volcano, Italy. *Journal of Geophysical Research: Solid Earth*, *113*(B9).

Spilliaert, N., Allard, P., Métrich, N. and Sobolev, A.V., 2006. Melt inclusion record of the conditions of ascent, degassing, and extrusion of volatile-rich alkali basalt during the powerful 2002 flank eruption of Mount Etna (Italy). *Journal of Geophysical Research: Solid Earth*, *111*(B4).

Steffke, A.M., Harris, A.J.L., Burton, M., Caltabiano, T., Salerno, G.G., 2011. Coupled use of COSPEC and satellite measurements to define the volumetric balance during effusive eruptions at Mt. Etna, Italy. *Journal of Volcanology and Geothermal Research*, 205(1–2):47-53.

Symonds, R.B., Gerlach, T.M. and Reed, M.H., 2001. Magmatic gas scrubbing: implications for volcano monitoring. *Journal of Volcanology and Geothermal Research*, *108*(1-4), pp.303-341.

Tanguy, J.C., Condomines, M. and Kieffer, G., 1997. Evolution of the Mount Etna magma: constraints on the present feeding system and eruptive mechanism. *Journal of Volcanology and Geothermal research*, *75*(3-4), pp.221-250.

Tonarini, S., Armienti, P., D'Orazio, M., Innocenti, F., Pompilio, M., and Petrini, R., 1995, Geochemical and isotopic monitoring of Mt. Etna 1989–1993 eruptive activity: bearing on the shallow feeding system: Journal of Volcanology and Geothermal Research, v. 64, p. 95–115, doi:10.1016/0377-0273(94)00039-J.

Venugopal, S., Schiavi, F., Moune, S., Bolfan-Casanova, N., Druitt, T. and Williams-Jones, G., 2020. Melt inclusion vapour bubbles: the hidden reservoir for major and volatile elements. *Scientific reports*, *10*(1), pp.1-14.

Viccaro, M., Calcagno, R., Garozzo, I., Giuffrida, M., and Nicotra, E., 2015, Continuous magma recharge at Mt. Etna during the 2011–2013 period controls the style of volcanic activity and compositions of erupted lavas: Mineralogy and Petrology, v. 109, p. 67–83, doi:10.1007/s00710-014-0352-4.

Viccaro, M., and Cristofolini, R., 2008, Nature of mantle heterogeneity and its role in the short-term geochemical and volcanological evolution of Mt. Etna (Italy): Lithos, v. 105, p. 272–288, doi:10.1016/j.lithos.2008.05.001.

Wallace, L.M., Beavan, J., McCaffrey, R. and Darby, D., 2004. Subduction zone coupling and tectonic block rotations in the North Island, New Zealand. *Journal of Geophysical Research: Solid Earth*, *109*(B12).

Wallace, P.J., 2003. From mantle to atmosphere: magma degassing, explosive eruptions, and volcanic volatile budgets. In *Developments in volcanology* (Vol. 5, pp. 105-127). Elsevier.

Wallace, P.J., 2005. Volatiles in subduction zone magmas: concentrations and fluxes based on melt inclusion and volcanic gas data. *Journal of volcanology and Geothermal Research*, *140*(1-3), pp.217-240.

Wallace, P.J. and Edmonds, M., 2011. The sulfur budget in magmas: evidence from melt inclusions, submarine glasses, and volcanic gas emissions. *Reviews in Mineralogy and Geochemistry*, *73*(1), pp.215-246.

Wallace, P.J., Kamenetsky, V.S. and Cervantes, P., 2015. Melt inclusion CO2 contents, pressures of olivine crystallization, and the problem of shrinkage bubbles. *American Mineralogist*, *100*(4), pp.787-794.

Wardell, L.J., Kyle, P.R., Dunbar, N. and Christenson, B., 2001. White Island volcano, New Zealand: carbon dioxide and sulfur dioxide emission rates and melt inclusion studies. *Chemical Geology*, *177*(1-2), pp.187-200.

Wieser, P.E., Iacovino, K., Matthews, S, Moore, G.M., and Allison, C. (2022). VESIcal Part II: A critical approach to volatile solubility modelling using an open-source Python3 engine. *Earth and Space Sciences.*

Werner, C.A., Doukas, M.P. and Kelly, P.J., 2011. Gas emissions from failed and actual eruptions from Cook Inlet Volcanoes, Alaska, 1989–2006. *Bulletin of Volcanology*, *73*(2), pp.155-173.

Williams, S.N., Schaefer, S.J., Calvache, V.M.L. and Lopez, D., 1992. Global carbon dioxide emission to the atmosphere by volcanoes. *Geochimica et Cosmochimica Acta*, *56*(4), pp.1765-1770.

Witham, F., Blundy, J., Kohn, S.C., Lesne, P., Dixon, J., Churakov, S.V. and Botcharnikov, R., 2012. SolEx: A model for mixed COHSCl-volatile solubilities and exsolved gas compositions in basalt. *Computers & Geosciences*, *45*, pp.87-97.

Wolery, T J. EQ3/6, a software package for geochemical modeling of aqueous systems: Package overview and installation guide (Version 7.0). United States: N. p., 1992. Web. doi:10.2172/138894.

Wolery, T.J. and Daveler, S.A., 1992. *EQ6, a computer program for reaction path modeling of aqueous geochemical systems: Theoretical manual, users guide, and related documentation (Version 7.0); Part 4* (No. UCRL-MA-110662-Pt. 4). Lawrence Livermore National Lab., CA (United States).

Zheng, Y.F. and Hoefs, J., 1993. Effects of mineral precipitation on the sulfur isotope composition of hydrothermal solutions. *Chemical Geology*, *105*(4), pp.259-269.